Energy dissipation in prestressed concrete beams
by Khimji N Vira

A thesis Submitted to the Graduate Faculty in partial fulfillment of the requirements for the degree of MASTER OF SCIENCE in Civil Engineering
Montana State University

Abstract:
An apparatus was designed and fabricated to investigate the damping properties of prestressed concrete beams.

Ten prestressed concrete beams 6” wide by 3" deep by 78" long, having prestress cables in the center, were tested under repeated reversible static loading. The equivalent viscous, damping ratio, determined from the area within the resulting hysteresis loops, did not exceed 4% critical even when the beams were close to failure.

The equivalent viscous damping ratio, determined from steady state vibrations and also from the decay of free vibrations, did not exceed 5% critical. After the beams had been loaded past the point of deterioration the equivalent viscous damping ratio was as high as

ENERGY DISSIPATION IN PRESTRESSED CONCRETE BEAMS

by

KHIMJI N. VIRA

A thesis submitted to the Graduate Faculty in partial fulfillment of the requirements for the degree

of

MASTER OF SCIENCE

in

Civil Engineering

Approved:

Head, Major Department

Chairman, Examining Committee

Dean, Graduate Division

MONTANA STATE COLLEGE
Bozeman, Montana

March, 1964

ACKNOWLEDGEMENT

The author wishes to express his appreciation and sincere thanks to all those individuals who have assisted in this study. He would like especially to thank Dr. W. O. Keightley for his guidance and many helpful suggestions. He is also thankful to Professor Martin Moss for his guidance and advice.

The facilities and the funds for the materials for this work were provided by the Civil Engineering and Mechanics Department. Laboratory facilities were also provided by the Mechanical Engineering Department. Thanks are extended to the Ideal Cement Plant at Trident, Montana, for donating the cement.

Finally, thanks are due to Mr. and Mrs. Robert Romanowski for their assistance in typing this thesis.

TABLE OF CONTENTS

TABLE OF CONTENTS (Cont.)

LIST OF TABLES

LIST OF FIGURES

LIST OF FIGURES (Cont.)

ABSTRACT

An apparatus was designed and fabricated to investigate the damping properties of prestressed concrete beams.

Ten prestressed concrete beams 6" wide by 3" deep by 78" long, having prestress cables in the center, were tested under repeated reversible static loading. The equivalent viscous damping ratio, determined from the area within the resulting hysteresis loops, did not exceed 4% critical even when the beams were close to failure. The equivalent viscous damping ratio, determined from steady state vibrations and also from the decay of free vibrations, did not exceed 5% critical. After the beams had been loaded past the point of deterioration the equivalent viscous damping ratio was as high as 7%.

CHAPTER 1

INTRODUCTION

In recent years the behavior of structures subjected to various types of dynamic loading conditions has become the subject of much investigation. These dynamic loading conditions may be produced by earthquake loading, blast loading, wind loading, impact loading due to traffic, or by the operation of unbalanced machinery. To predict the response of structures to dynamic excitation it is necessary to know the dynamic characteristics of the structural elements.

The primary objective of this investigation was to determine the damping characteristics of prestressed concrete beams and to compare the damping, determined from static measurements, with the damping determined from dynamic measurements. An apparatus was designed and fabricated to test simply supported prestressed concrete beams under repeated reversible static loads. The energy dissipation was determined by measuring the area within the resulting hysteresis loops. The dynamic damping was determined from the resonance curve produced by steady state excitation of the beams and by the rate of decay of the amplitude of free vibrations.

The primary emphasis was placed on the measurement of solid (static) energy dissipation and the apparatus was specially built for this purpose. The dynamic tests were complicated by the fact that portions of the support system were observed to be vibrating at amplitudes as high as one-half the amplitude at the center of the beam. Only a few beams were tested dynamically to attempt to find some correlation with the static test.

The experimental investigation reported herein was undertaken with the primary objectives of determining:

1. If the mix design strength of concrete affects damping.
2. If air entrained in the concrete affects damping.
3. Whether badly cracked beams dissipate more energy than uncracked beams undergoing the same displacement cycle.
4. If a relationship can be found between static damping and dynamic damping.
5. If grouting of the prestressed cables in the beam affects the damping.

CHAPTER 2

REVIEW OF THE LITERATURE

2.1 HISTORICAL BACKGROUND

Research on the damping properties of materials and their engineering significance was started almost two hundred years ago. One of the early pioneers in this field was Coulomb. In 1784, he hypothesized a micro-structure mechanism of damping and also conducted research and concluded that the damping of torsional oscillations is not caused by air friction, but it is due to internal losses in the material (1)*.

Intensive work on hysteresis damping was not started until the end of the 19th century. Work on the hysteretic effect under cyclic stress was done by Ewing (1) in 1889. Work on hysteresis damping under cyclic bending was started by Voight (1) in 1892.

More recent studies on the behavior of structural elements under impulsive loading were undertaken at the Massachusetts Institute of Technology in 1951. It was established there that conventional concrete beams absorb 30% more energy under dynamic loading (impulsive loading) than under reversible static loading (2).

Work done at the United States Naval Civil Engineering Laboratory at Port Hueneme, California, revealed that the damping ratio decreased with the decrease of load duration. The load duration was defined as

---

*Numbers in brackets refer to references on page 74. (LITERATURE CITED) the ratio of actual (effective) load duration to the natural period of the beam (3).

In 1962, Penzien (4) concluded from dynamic tests that damping in prestressed concrete beams increases with the development of large cracks, from 2% at low stresses to 6% at stresses close to failure, and so the magnitude and type of prestress in the concrete member has an indirect effect on the damping.

2.2 TYPES OF DAMPING

Damping is a complex mechanism. Many investigators have tried to develop different types of simple equations and simple mechanisms to represent damping. Damping can be classified as:

1. Damping dependent on velocity.
2. Damping independent of velocity.

2.2.1 DAMPING DEPENDENT ON VELOCITY

Viscous damping is included in this classification. The concept of viscous damping has been known to the world for hundreds of years. Viscous damping is represented by a simple mechanism, based on the concept that damping forces are proportional to the velocity of the vibrating system.

Figure 1 represents a system that is subjected to harmonic force $F_o \sin \omega t$. The mass, m, is suspended on a linear spring of stiffness, k, in parallel to the dashpot that provides viscous damping with a factor c. This dashpot opposes the motion of the mass with a force,

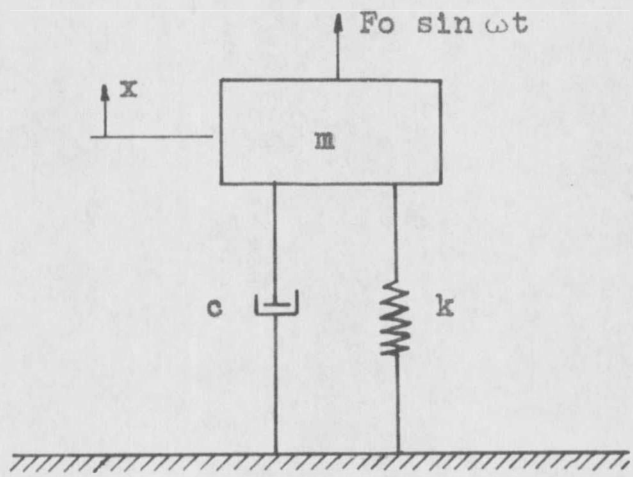

Figure 1: One-degree-of-freedom system with viscous damper.

$c\dot{x}$, where x is measured from the equilibrium position of the mass (5).

Summing the forces on the mass the following equation is derived:

$$m\ddot{x} + c\dot{x} + kx = Fo \sin \omega t \quad \ldots \ldots \quad 1$$

If the steady state response is

$$x = a \sin(\omega t - \phi)$$

where a is the amplitude of vibration and ϕ is the phase angle, the net work input per cycle, ΔE, at steady state is

$$\Delta E = \int (\text{force})\, dx$$

$$= \int_0^{\tau} (Fo \sin \omega t)\, \dot{x}\, dt$$

$$= \omega Fo\, a \int_0^{\tau} \sin \omega t \cos(\omega t - \phi)\, dt$$

$$= Fo\, a \int_0^{2\pi} \sin \omega t \cos(\omega t - \phi)\, d(\omega t)$$

$$= Fo\, a\, \pi \sin \phi \quad \ldots \ldots \quad 2$$

where τ is the period of vibration.

When the force is in phase or 180° out of phase with the displacement, the work done per cycle is zero. The work done per cycle is maximum when the phase angle is 90°. Thus the harmonic force $Fo \sin \omega t$ can be separated into two parts, one in phase or 180° out of phase with displacement, x, and other 90° out of phase with the displacement.

The energy dissipation per cycle, ΔE, due to the damping force is

$$\Delta E = \int (\text{damping force})\, dx$$

$$= \int_0^{\tau} (\text{damping force})\, \dot{x}\, dt$$

In a system with viscous damping this energy dissipation is

$$\Delta E = \int_0^{T} (c\dot{x})\ \dot{x}\ dt$$
$$= \int_0^{T} c\,\omega^2 a^2 \cos^2(\omega t - \phi)\ dt$$
$$= c\,\omega\pi a^2 \qquad \ldots\ldots\ldots\ldots\ 3$$

By equating the net work input to the energy dissipation per cycle

$$Fo\ a\ \pi \sin\phi = c\omega\pi a^2$$
$$a = \frac{Fo \sin\phi}{c\,\omega}$$

At natural frequency of the system, ω_n, $\sin\phi = 1$ and

$$a = \frac{Fo}{c\,\omega_n}$$

Thus the amplitude of the system is inversely proportional to the damping constant.

A strong reason for the popularity of the viscous damping concept is that it does not destroy the linearity of the differential equation describing the motion.

2.2.2 DAMPING INDEPENDENT OF VELOCITY

Damping which is independent of velocity is also referred to as static damping. The concept of viscous damping, in which the energy absorption is proportional to the velocity, fails in the case of a system subjected to static loading irrespective of velocity. Several investigators have tried to develop mathematical concepts which permit energy dissipation independent of velocity.

Myklestad (6), in 1952, suggested that damping can be described mathematically by multiplying the modulus of elasticity of the material by complex number, e^{2bi}, where 2b is called the complex damping factor and i is $\sqrt{-1}$. Thus the equation of motion becomes

$$m\ddot{x} + k\,(1 + e^{2bi})\,x = F_o\,e^{i\omega t}$$

The damping force is always at 90° to the displacement, but it is independent of velocity.

Jennings (8), in 1963, developed a general nonlinear hysteretic force deflection relation for a one degree-of-freedom structure. He represented the force deflection relation by equation

$$\frac{x}{x_y} = \frac{p}{p_y} + \alpha\left(\frac{p}{p_y}\right)^r$$

where x is the displacement of the structure, x_y is a characteristic displacement, p is the restoring force, p_y is a characteristic force, α is a positive constant, and r is a positive integer greater than one. This formulation yields a hysteresis loop, the shapes of which depend on α and r, but which are independent of velocity.

Coulomb damping is independent of velocity. Coulomb damping, or dry friction damping, is the dissipation of energy that occurs when a particle in a vibrating system is resisted by a force whose magnitude is constant, independent of displacement and velocity and whose direction is opposite to the direction of the velocity of the particle (7).

2.2.3 EQUIVALENT VISCOUS DAMPING

The assumption here is that the actual nonlinear system may be approximated by a linear system with viscous damping. This concept of damping is frequently used to simplify the analysis of actual structural systems.

Nonviscous damping may be approximated by viscous damping by equating the energy dissipated in a nonviscous system to the energy dissipated in a viscous system.

$$\Delta E = c_{eq} \omega \pi a^2$$

where c_{eq} is the equivalent viscous damping coefficient. Since

$$c_{eq} = \frac{\Delta E}{\omega_n \pi a^2} \qquad \text{and} \qquad c_c = \frac{2k}{\omega_n}$$

where a system is vibrating at its natural frequency, ω_n, then

$$\zeta_{eq} = \frac{c_{eq}}{c_c} = \frac{\Delta E}{2\pi k a^2} \quad \ldots\ldots\ldots\ldots\ldots\ldots \quad 4$$

where ζ_{eq} is the equivalent viscous damping ratio and c_c is the critical damping constant*.

Equation No. 4 defines the equivalent damping ratio regardless of the type of damping mechanism involved.

2.3 HYSTERESIS LOOPS

Materials do not behave perfectly elastically even at very low

---

*Critical damping is defined physically as the minimum viscous damping that will restrain a displaced system to return to its equilibrium position without oscillation (7).

stresses. When a member is subjected to repeated loads, the stress-strain or load-deflection diagram forms a hysteresis loop as shown in Figure 2. For any type of cyclic stress this loop will be present, but in some cases it is too narrow to be noticed by conventional tests. The shape of this loop varies with the type of material and with the stress level reached (1).

Static damping depends on a stress-strain law which is independent of time, not sensitive to stress rate. In such a case the shape of the loop, and as a result the damping constant, is independent of frequency.

Table I shows the simplest representative mechanical models for each of the classified behaviors. In these models S is a spring having linear elasticity, D is a dashpot which produces a resisting force proportional to velocity and C is a Coulomb friction unit which produces a constant force whenever slip occurs within the units, the direction of force being opposite to the direction of motion (1).

TABLE I

CLASSIFICATION OF VARIOUS TYPES OF HYSTERETIC DAMPING OF MATERIALS

	TYPES OF DAMPING	
NAME USED HERE	DYNAMIC HYSTERESIS	STATIC HYSTERESIS
Other Names	Viscoelastic, rheological, & rate-dependent hysteresis	Plastic, plastic flow, plastic strain and rate-independent hysteresis
Nature of Stress-Strain Laws	Essentially linear. Differential equation involving stress, strain, and their time derivatives	Essentially nonlinear, but excludes time derivatives of stress or strain

Table I (cont.)

TYPES OF DAMPING

NAME USED HERE	DYNAMIC HYSTERESIS	STATIC HYSTERESIS	
Special Cases & Description	Anelasticity. Special because no permanent set after sufficient time. Called "internal friction"		
Simplest Representative Mechanical Model	Voigt unit, Maxwell unit 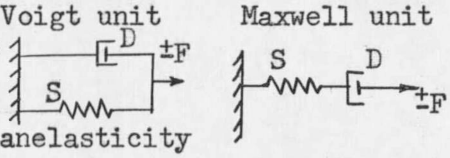 anelasticity	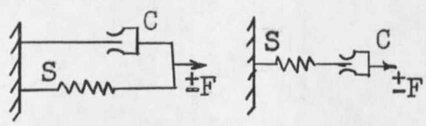	
Frequency Dependence	Critically at relaxation peaks	No, unless other mechanisms present	
Primary Mechanisms	Solute atoms, grain boundaries. Micro- and macro-thermal and eddy currents. Molecular curling and uncurling in polymers.	Magnetoelasticity	Plastic strain
Stress Range of Eng. Importance	Anelasticity - low stress Viscoelasticity - all stresses	Low and medium Sometimes high	Medium and high stress

Source: Structural Damping, J. E. Ruzicka, editor, ASME publication, 1959, p. 18.

2.4 IMPORTANCE OF DAMPING IN APPLIED SCIENCES

Damping characteristics of materials have been utilized widely for studying the internal micro- and submicro-structures of materials. Damping tests have also helped metallurgists to verify hypotheses on the structure and the anelastic mechanism of crystalline materials. Damping tests have also helped physical chemists to visualize the molecular structure of polymeric materials (1).

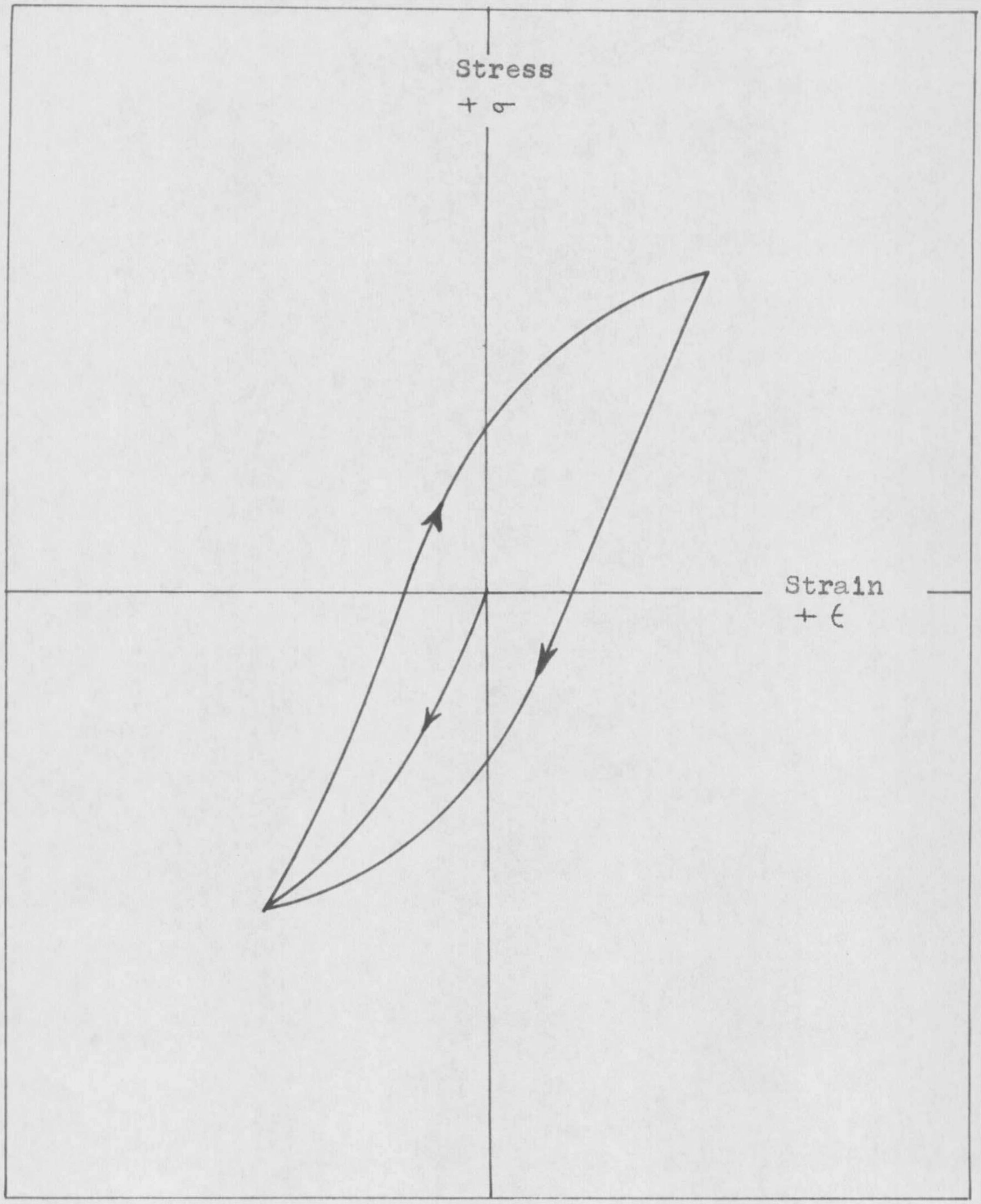

Figure 2: Typical stress-strain hysteresis loop.

In the engineering field the damping capacity of a material has been utilized as a significant property in the analysis of structural and acoustical performance. In the design of modern giant structures the damping characteristics play an important part. From the point of view of resistance to earthquake loads, the presence of a relatively large amount of damping in a structure is highly desirable because it dissipates the vibrational energy transmitted to the structure by the quake.

CHAPTER 3

EXPERIMENTAL PROGRAM

3.1 TEST SPECIMENS

The testing program consisted of tests on ten prestressed concrete beams 6" wide by 3" deep by 78" long. Table II in Appendix A summarizes the important features of each beam by giving the properties of the concrete and the prestress conditions just prior to testing.

3.2 PROPERTIES OF MATERIALS

3.2.1 CONCRETE

The mix designs were based on 0.8% and 2.7% moisture contents in the sand and in the gravel, respectively. These values were determined before the mixing operation began. A later determination of moisture contents showed the moisture in the sand had increased from 0.8% to 1.6% and the moisture in the gravel had decreased from 2.7% to 1.57%. Thus it is apparent that the water-cement ratio of the mixes was not precisely known.

BATCH 1

Beams numbered 1 to 4 were cast from this batch.

The designed ultimate compressive strength of 6" x 12" cylinders, after 28 days of moist curing at 70° F., was f'_c = 6000 pounds per square inch.

The proportions by weight of Type 1 Portland Cement, sand, gravel, and water used in the mix were 1.00 : 1.07 : 1.71 : 0.365. The measured slump was 3".

BATCH 2

Beams numbered 5 to 8 were cast from this batch.

The designed value of f_c' was 4000 pounds per square inch. The proportions by weight of Type 1 Portland Cement, sand, gravel, and water used in the mix were 1.0 : 2.13 : 2.7 : 0.56. The slump of this mix was 3".

BATCH 3

Beams numbered 9 and 10 were cast from this batch.

The designed value of f_c' was 4000 pounds per square inch. The proportions by weight of Type 1 Portland Cement, sand, gravel, and water used in the mix were 1.0 : 2.4 : 2.92 : 0.532. The slump of this mix was 3". Air, 5.2% of the volume of the mix, was entrained by adding 6 cc. of Protex per sack of cement used in the batch.

3.2.2 CEMENT

The cement used in the concrete was Type 1 Portland Cement, manufactured and donated for this project by the Ideal Cement Plant at Trident, Montana. A chemical analysis furnished by the company is in Appendix B.

3.2.3 SAND

The sand, termed Gallatin sand, was obtained locally from a pit near Interstate Highway 10, close to Belgrade, Montana. It was washed and graded to meet ASTM specification C 33-54T.

The bulk specific gravity on the basis of saturated surface dry aggregate and the absorption, determined by ASTM Standard Method C 128-42 were 2.62 and 1.6% respectively. The fineness modulus was determined to be 2.79.

The gradation is presented in Appendix C.

3.2.4 GRAVEL

The gravel was obtained from the same pit from which the sand had come. It was washed and graded to meet ASTM Specification C 33-54T.

The maximum size of the gravel was $\frac{3}{4}$". The bulk specific gravity on the basis of saturated surface-dry aggregate and the absorption, determined by ASTM Standard Method C 127-42, were 2.60 and 1.35%, respectively. The gradation is presented in Appendix C.

3.2.5 PRESTRESS CABLE

The prestress cable consisted of seven wires, each $\frac{1}{10}$" in diameter. The nominal size of the cable was $\frac{5}{16}$" diameter.

The stress-strain characteristics and the other properties of the cable are not known.

3.3 CASTING BEAMS

Materials for the concrete were weighed out and introduced into a Lancaster Counter Current Rapid Batch Mixer, Model SKG, $1\frac{3}{4}$ cubic feet capacity, sufficient to cast two beams. The beams were then cast side by side in oiled wooden forms, consisting of a plywood base and 1" thick boards to form the sides and ends of the beams. To provide the passage for the prestress cables, two flexible galvanized conduits, $\frac{1}{2}$" diameter, were embedded in the beams as shown in Table II, Appendix A. The beams were left in their forms for the first 24 hours and then were placed in a fog room at a temperature around 70° F. The curing periods for the beams varied from 8 to 12 weeks, depending upon the testing schedule.

Three standard control cyclinders, 6" x 12", were cast along with each batch from the mixer and were cured in a manner similar to that of the beams.

Post-tensioning of each beam was started within a few hours after the beam was removed from the fog room. Tensioning of the cables was accomplished with a Simplex Center Hole Ram and a Simplex Hydraulic Four-Way Jack. Steel bearing plates, $\frac{3}{4}$" in thickness, were used at each end of the beams. Gifford-Udall chucks were used to grip the cables. Tensioning of the cables was achieved by tensioning the first cable to 2000 pounds and then the second cable to 4000 pounds, then the first cable to 6000 pounds, etc. This was repeated until the required tension, 7000 pounds, in each of the cables was achieved. The beam was tested within a few hours after the post-tensioning operation.

The cables in two of the beams having a design strength of 4000 pounds per square inch were grouted with a plain mortar grout composed of Type 1 cement and water in the proportions 1.0 : 0.42 by weight. In addition Pozzolith, 0.25% of the weight of cement, was added. The beams were placed in a slightly inclined position and the grout was forced by air pressure into the lower ends of the conduits. The beams were post-tensioned immediately after the grouting operation and then were left to air cure for 21 days before testing.

The faces of the beam contacting the support bearing plates and the loading clamps were made smooth by capping the top and the bottom faces of the beam, at the ends and at the center, with a sulphur compound normally used for capping control test cylinders.

3.4 STATIC TESTING APPARATUS

Figure 3 shows a general view of the apparatus used in this research for testing beams under repeated reversible loads. The primary objective of designing and building this apparatus was to record the dissipated energy in a beam under one cycle of reversible load. The apparatus was not ideal but the design was carefully examined and the apparatus was modified to eliminate imperfections as far as possible.

The description of the apparatus is divided into five parts:

1. Beam supports.
2. Deflection measuring device.
3. Loading device and load recording equipment.
4. Dynamic testing equipment.

3.4.1 BEAM SUPPORTS

Figure 4 shows a close and detailed view of one support. Each

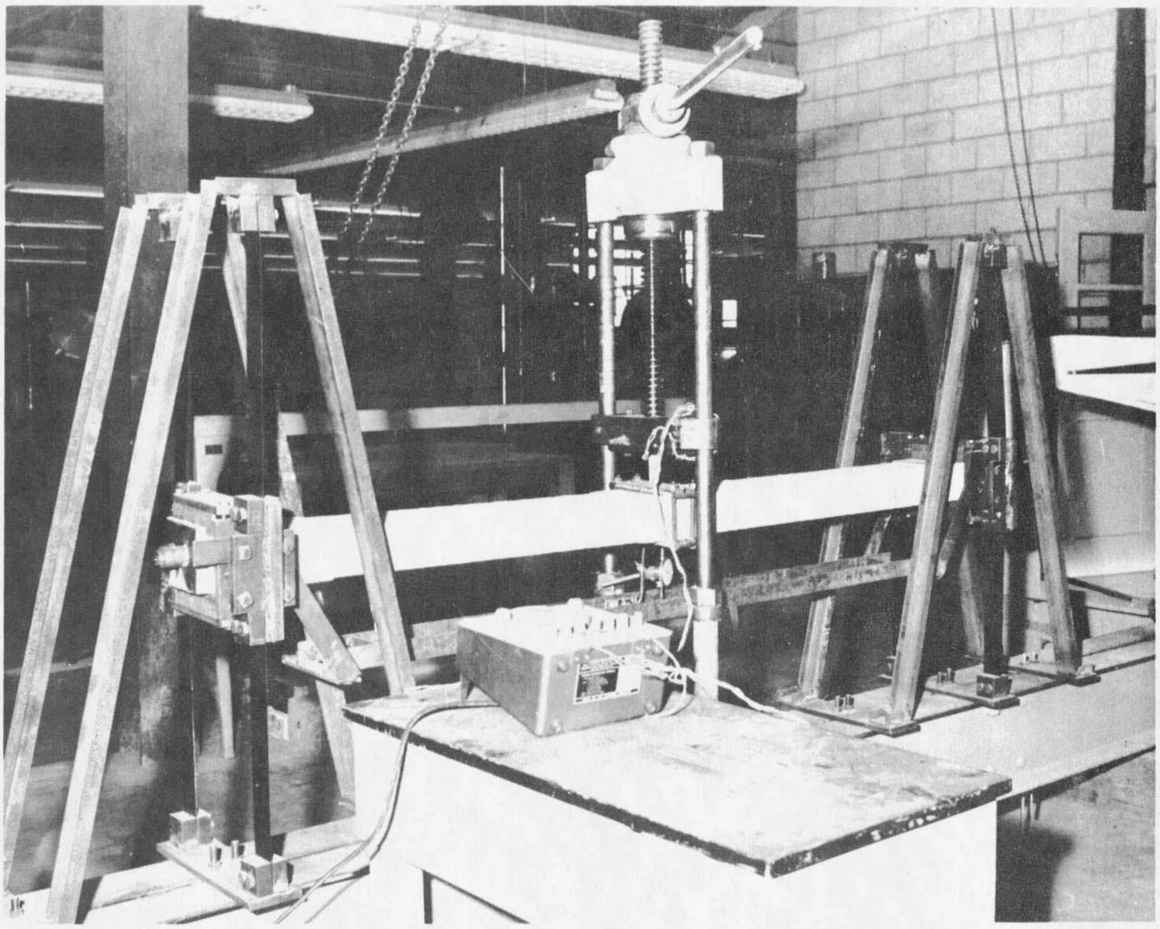

Figure 3: General view of the static testing apparatus.

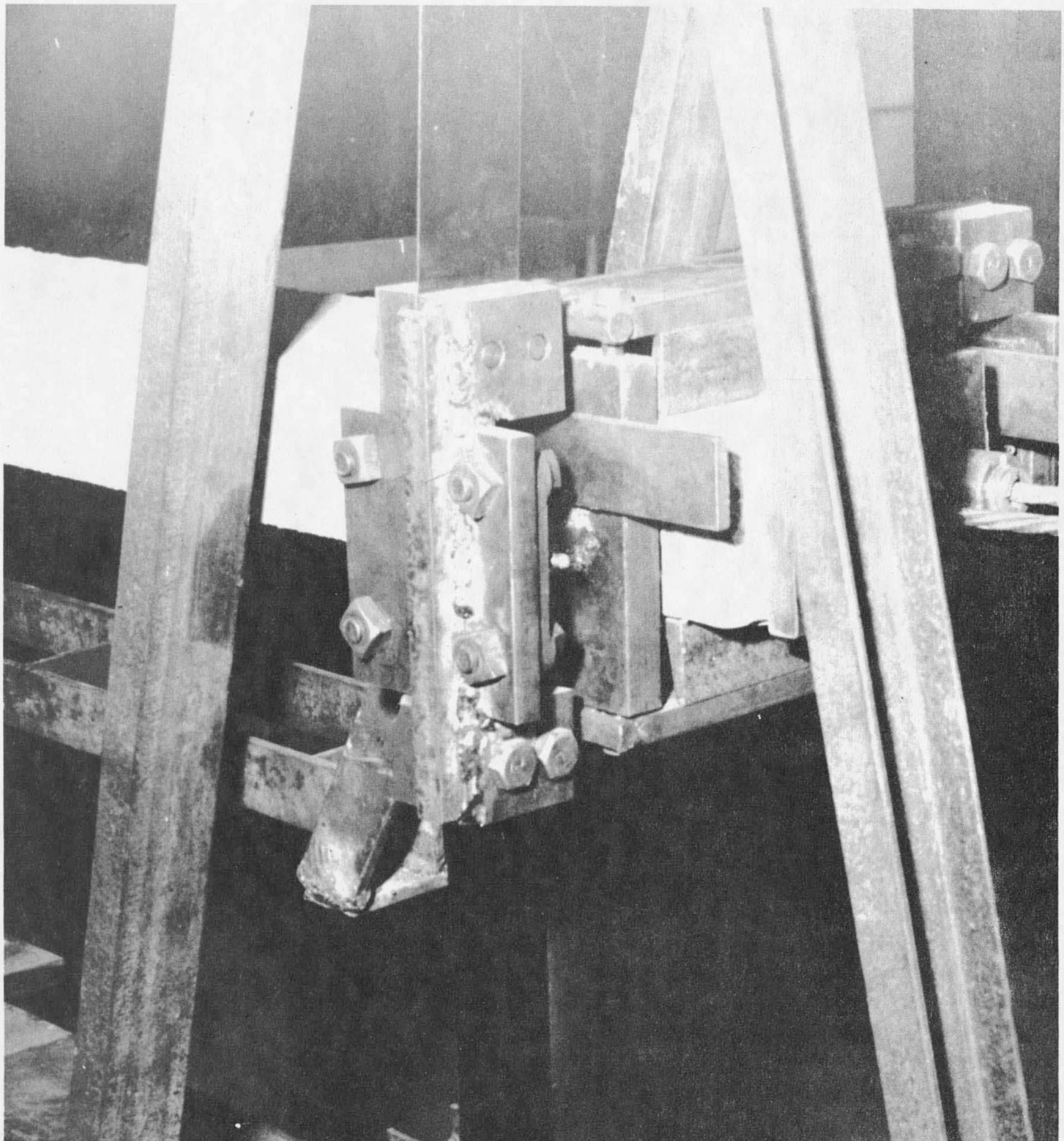

Figure 4: Detailed view of the beam support.

end of the beam was clamped by two steel bearing plates, 8" x 3" x $\frac{1}{4}$", one on the top face of the beam and the other at the bottom face. These bearing plates were bolted tightly to steel side plates, 5" x 3" x $\frac{1}{2}$", from each of which extended a 1" diameter steel shaft, 3" long. The whole clamp at the end of the beam was supported by these shafts which in turn extended into bronze bearings on each side of the beam, as shown in Figure 5.

The bronze bearings were used in the construction so that the end of the beam could rotate with very small restraining moments and thus maintain the energy loss in the supports at a very low value.

The bronze bearings, shown in Figure 6, were attached, top and bottom, to spring steel bands 16" long by 2" wide by $\frac{1}{32}$" thick. The purpose of the spring steel bands was to provide vertical reactions at the end of the beam with only very small accompanying end moments. The bands also allowed the ends of the beam to move in the longitudinal direction to accommodate the shortening of the neutral axis. It can be shown that practically no end moments were distributed in the bands. This type of support effectively provided the concrete beam with simply supported ends.

The entire assembly was attached to a frame, made of steel channel, 2" deep by 4.1 pounds per foot, as shown in Figure 2. The frames were mounted on the base of a beam testing machine which consisted of two I beams, 10" by $5\frac{3}{4}$" size, 12' long, spaced $5\frac{1}{4}$" center to center.

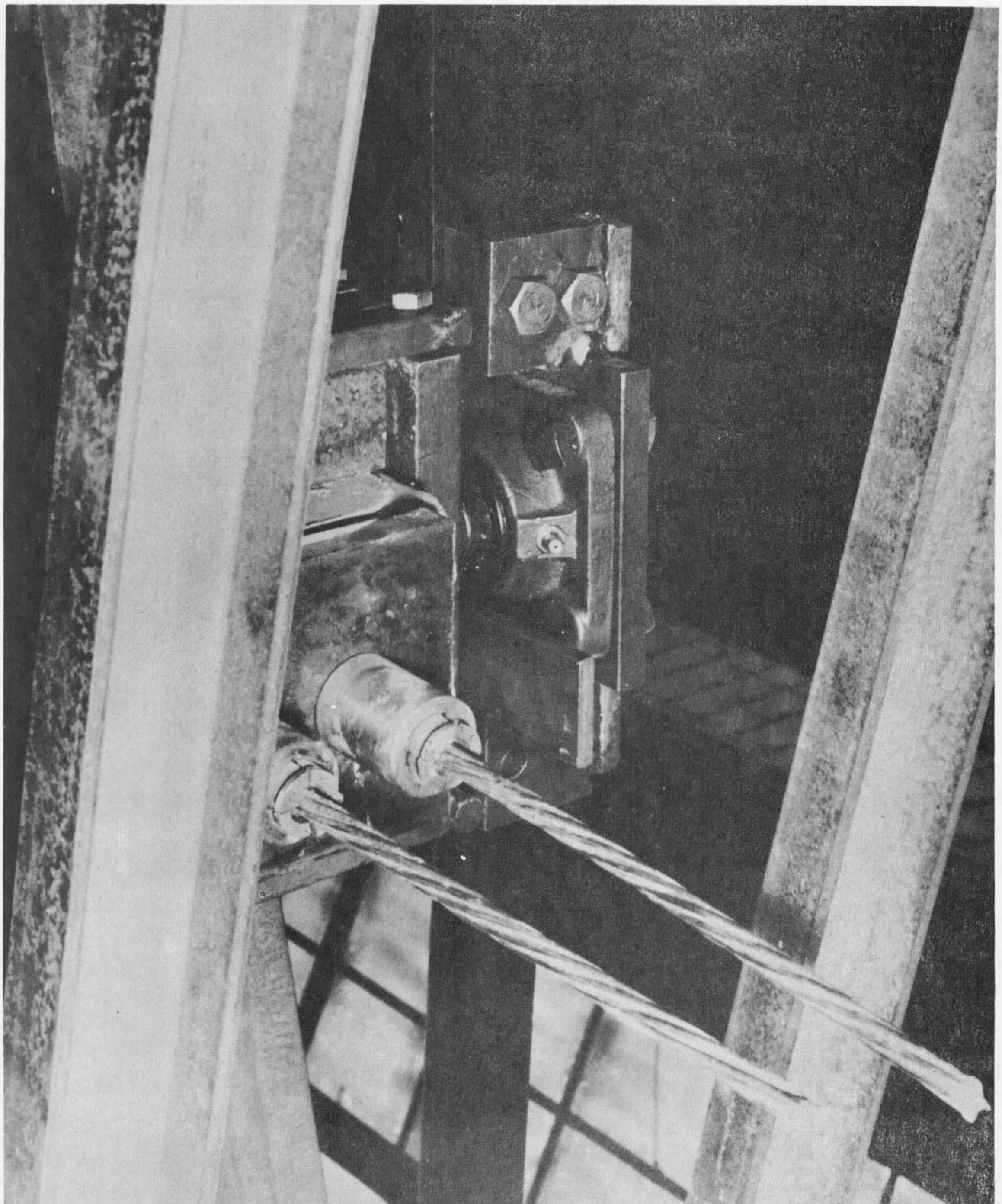

Figure 5: Detailed view of the support clamp.

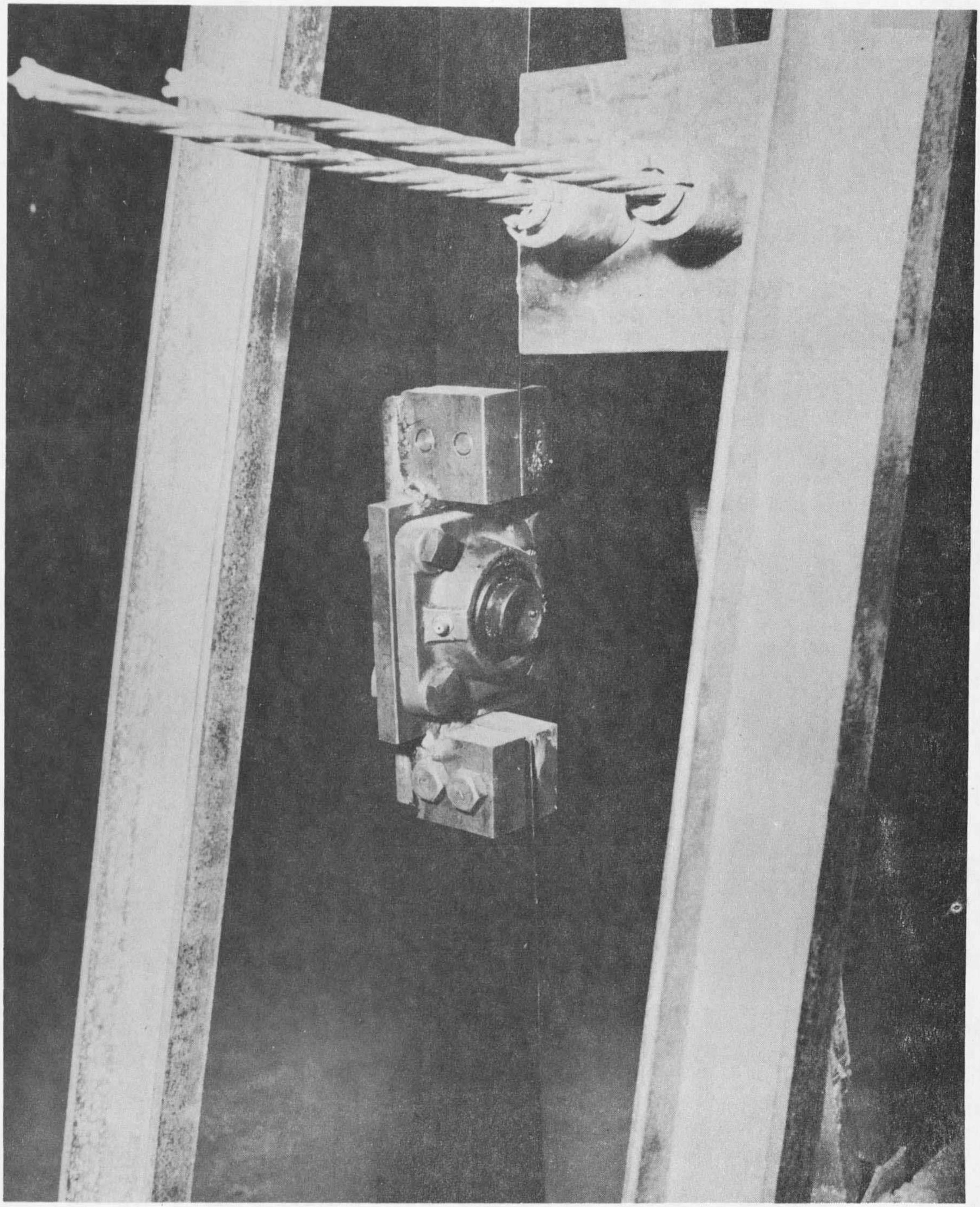

Figure 6: Detailed view of the bronze-bearing.

3.4.2 DEFLECTION MEASURING DEVICE

The bridge assembly was used for measuring deflections of the beams. The bridge consisted of steel strips welded as shown in Figure 7. Each end of the bridge rested on the shafts extending from the side plates. The contacts between the shafts and the ends of the bridge were lubricated with graphite grease to reduce energy loss when the shafts rotated as the beam was loaded.

The deflections of the centerline of the beam, relative to the neutral axis at the supports, were measured with an Ames dial guage, type 282, with a least division of 0.001 inch and a travel of one inch. The base of the gauge was attached to the center of the bridge by means of a magnetic clamp directly below the line of action of the load. The tip of the shaft of the gauge was cemented to the bottom plate of the loading system clamp.

3.4.3 LOADING DEVICE

The loading device, shown in Figure 3, consisted of a vertical screw, two threads per inch, passing through a yoke which was mounted above the beam. By manually turning a long handle extending from a threaded collar attached to the yoke, it was possible to cause both upward and downward displacement of the center of the beam. The loading head was attached to the center of the beam by two steel plates, 8" long by 3" wide by $\frac{1}{2}$" thick, which clamped the beam, one on the top face of the beam and the other at the bottom face of the

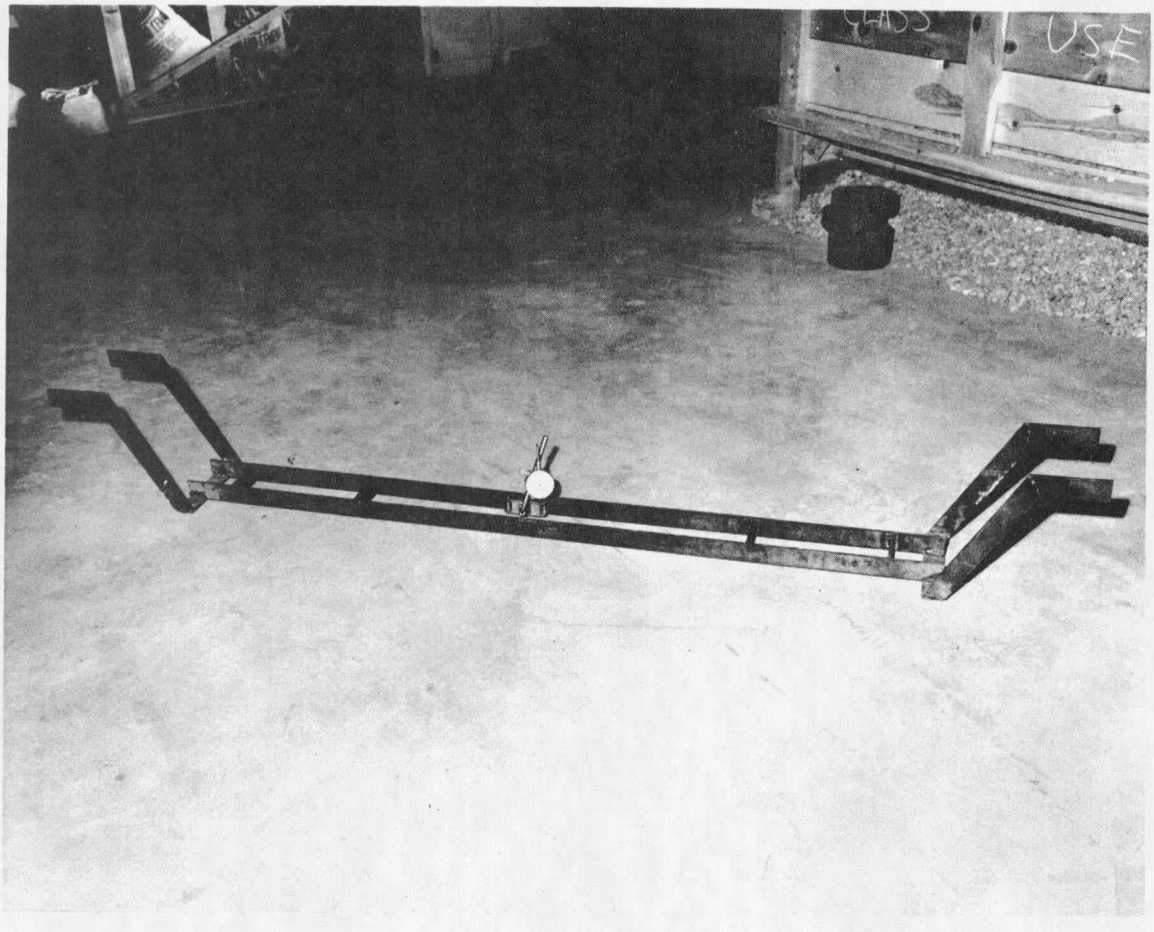

Figure 7: Deflection measuring device.

beam.

The clamps were secured to the loading head by a force transducer capable of carrying both tensile and compressive loads. The force gauge was an aluminum rod, type 2024 T4, $\frac{1}{2}$" diameter by 3" long threaded at the top and bottom, respectively, into the loading head and the top plate of the loading clamps. Two electric resistance strain-gauges, Baldwin-Lima-Hamilton SR-4, type A-12, gauge factor 2.07, were cemented to the force transducer, diametrically opposite as shown in Figure 8.

The gauges were oriented so that a plane containing the axes of both gauges was perpendicular to the longitudinal axes of the beam. With the gauges connected in series in the bridge circuit as shown in Figure 8, the effects of bending of the force transducer were thus eliminated. The output of the bridge was measured with a Baldwin-Lima-Hamilton static strain indicator Type N.

Calibration of the force-transducer was accomplished by loading the unit in compression in a Baldwin-Lima-Hamilton 200,000 pounds capacity hydraulic testing machine. The calibration curve is shown in Appendix D. As a check, a dead load of 250 pounds was hung from the force transducer when it was mounted in the beam testing machine and the calibration was confirmed. No calibration of the force transducer in tension was attempted.

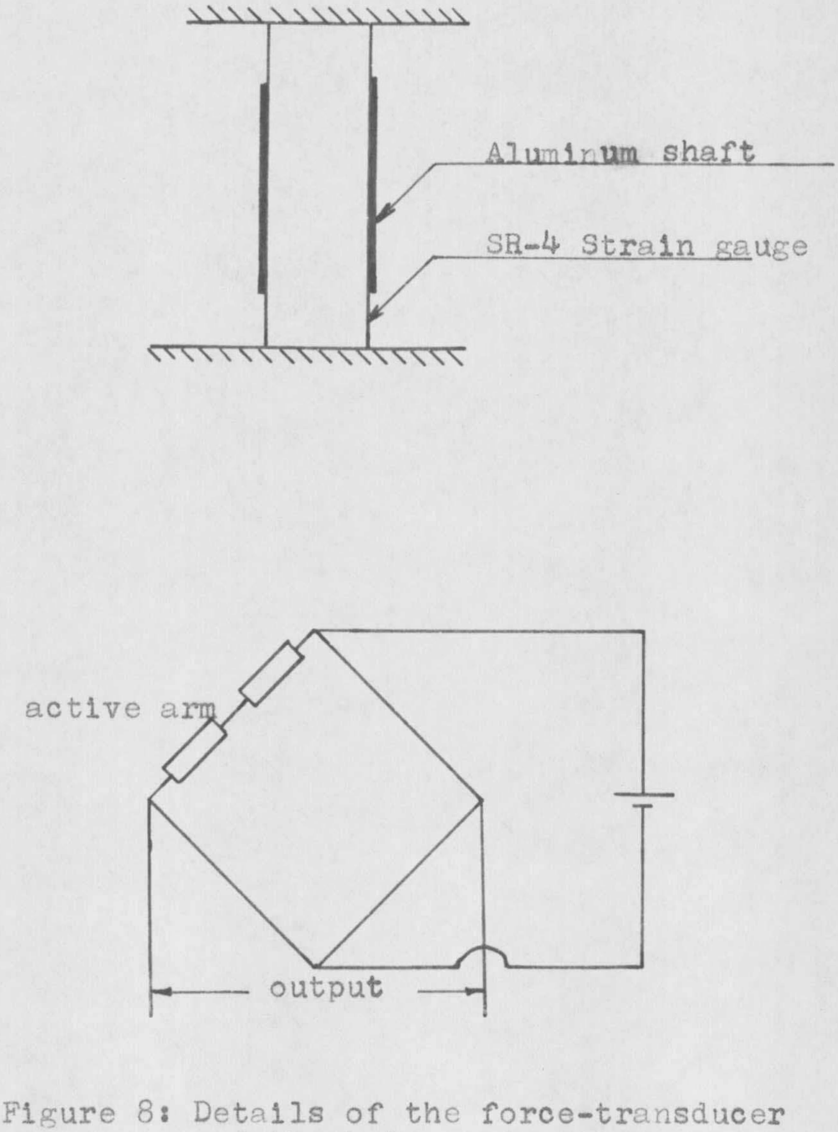

Figure 8: Details of the force-transducer
and the bridge circuit.

3.5 DYNAMIC TESTING EQUIPMENT

The dynamic testing equipment, shown in Figure 9, consisted of these main components:

1. The vibration exciter.
2. The frequency measuring system.
3. The amplitude recording system.

3.5.1 THE VIBRATION EXCITER

Figure 10 shows the mechanical vibrator. It consisted of a variable speed electric motor of $\frac{1}{32}$ H.P. size, on the shaft of which was mounted a metal disc with an eccentric mass. The voltage to the motor was controlled by a powerstat so that the speed of the motor could be varied continuously from zero to approximately 42 cycles per second.

Rotation of the eccentric mass resulted in an inertia force applied to the beam given by

$$F_V = m\omega^2 r \cos \omega t$$

$$F_H = m\omega^2 r \sin \omega t$$

where F_V and F_H are the vertical and horizontal forces, respectively, m is the eccentric mass, approximately 0.03 pound, r is the radius of rotation of mass, approximately 1.5", and ω is the angular velocity of eccentric mass.

The motor was mounted approximately 2" longitudinally from the centerline of the beam. Maximum amplitude of the beam itself at the point at which the motor was mounted was only 0.01", whereas the

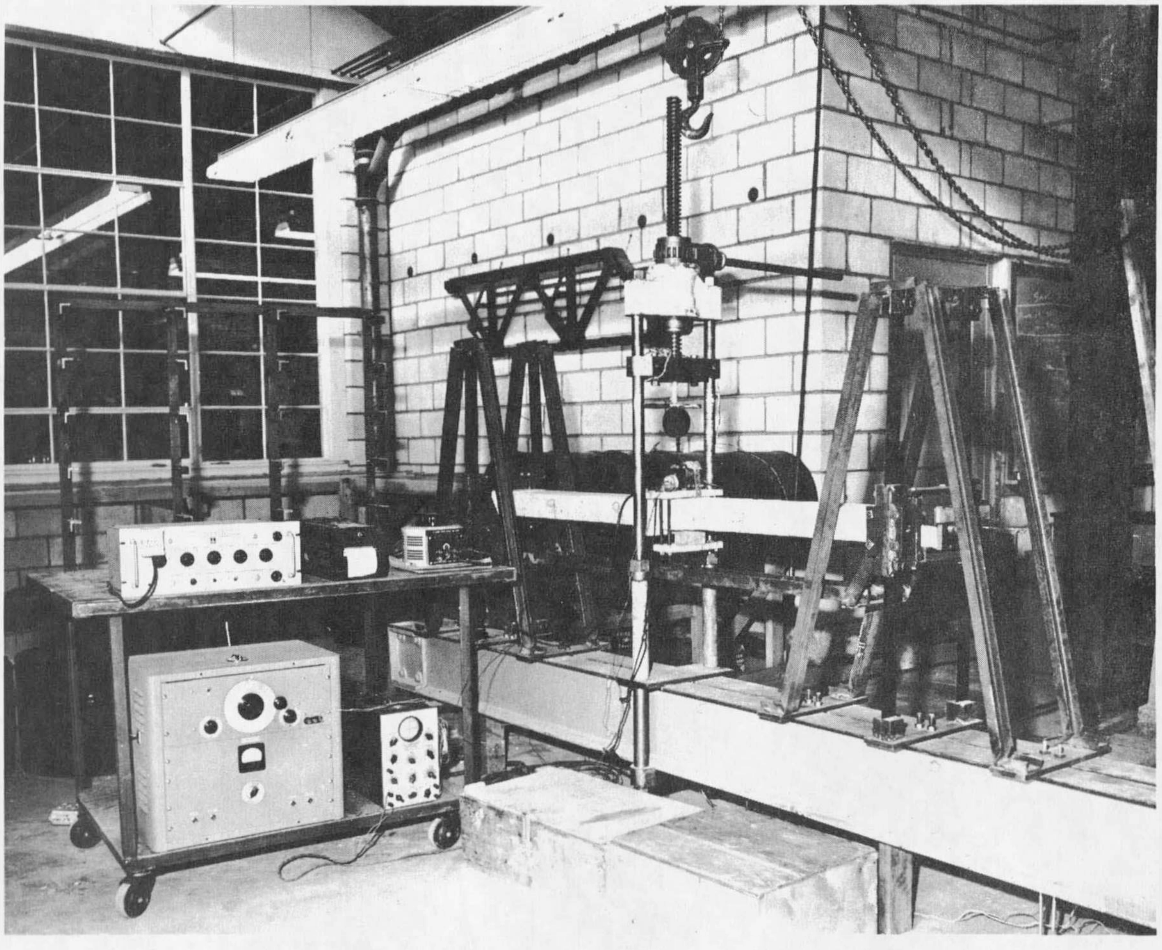

Figure 9: Dynamic testing equipment.

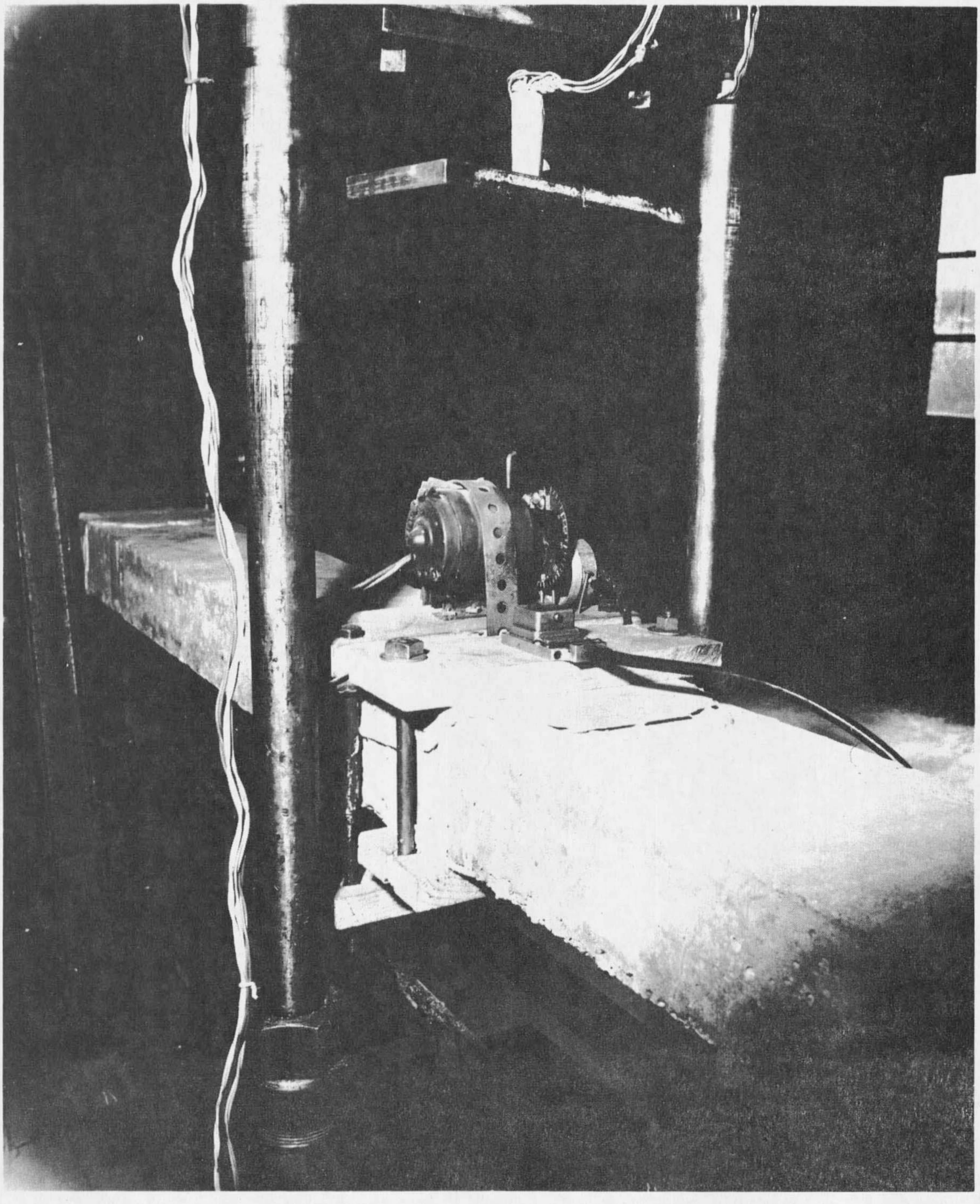

Figure 10: Details of the mechanical vibrator.

eccentricity of the mass from the shaft of the motor was 1.5". Thus it is apparent that the sinusoidal force applied to the beam was only slightly affected by the motion of the beam.

It is apparent from Figure 11 that the vertical force excites principally the first mode of vibration and the moment excites principally the second mode of vibration. Inasmuch as all the measurements were made close to the frequency of the first mode, and the location of the accelerometer was near the center of the beam, it is clear that the measurements were not affected by the movement caused by the horizontal inertia force to any significant extent.

Inasmuch as the frequency of longitudinal vibration of the beam was only two cycles per second, and the frequency of excitation of the of the beam was around 30 cycles per second, only small horizontal motion of the beam occurred. The records of the vertical vibrations were not affected by this horizontal motion of the beam because the accelerometer was mounted to record only vertical motion of the beam.

3.5.2 FREQUENCY MEASURING SYSTEM

The frequency measuring instruments are shown in Figure 12. When the eccentric mass passed through the magnetic field of the earphone mounted adjacent to the rotating disc, Figure 10, a pulse of electric current was generated once per cycle in the windings of the earphone magnet. This pulse was fed into the vertical axis of the cathode ray oscilloscope shown in Figure 12. The horizontal axis of the oscilloscope was driven by a sinusoidal voltage from the oscillator of an

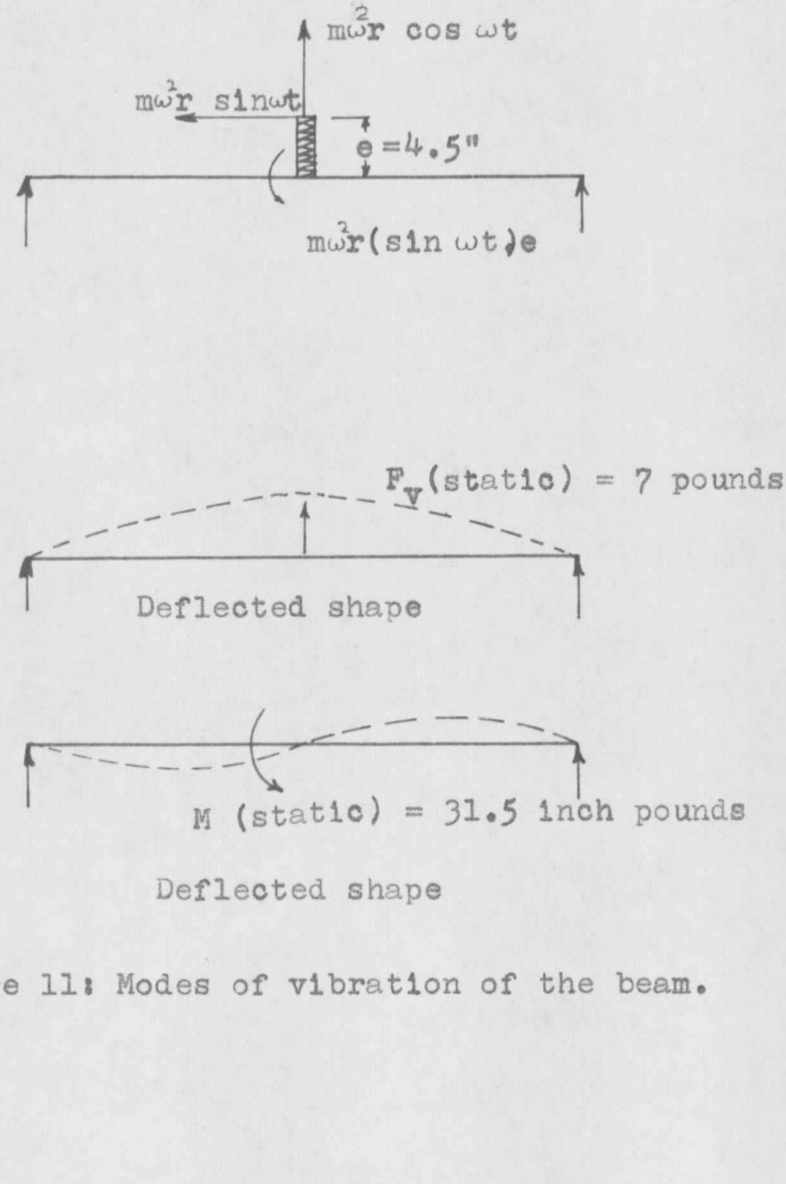

Figure 11: Modes of vibration of the beam.

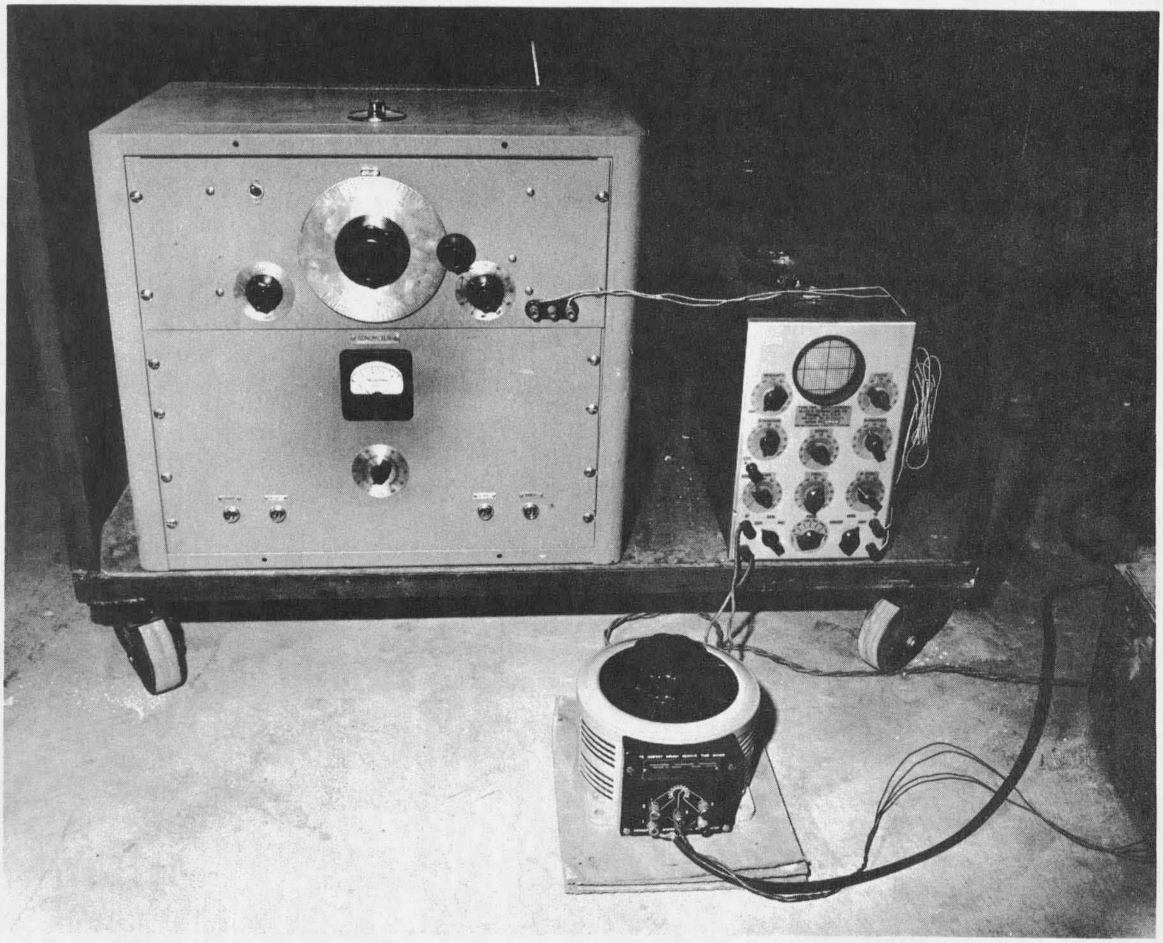

Figure 12: The frequency measuring instruments.

Electro Products Laboratories Inc. sonometer, model CT-360. The image of the pulse appeared to be stationary on the screen of the oscilloscope when the frequency of the signal from the sonometer was an integral multiple of the frequency of the pulse. The lowest frequency at which the image of the pulse remained stationary was taken to be the frequency of the forced vibrations of the beam.

3.5.3 THE AMPLITUDE RECORDING SYSTEM

The accelerations of the vibrating beam were recorded on a two-channel Brush Instruments Company Type BL 202 Direct Ink Writing oscillograph recorder with a Brush model BL 360 Carrier type amplifier input shown in Figure 13. The acceleration transducer used was the William Miller Company Type 402 C variable reluctance accelerometer. The accelerometer was mounted approximately one inch from the center-line of the beam to measure the vertical acceleration.

The overall calibrations of the accelerometer-amplifier-recording system were obtained by detaching the accelerometer from the beam and rotating the accelerometer about a horizontal axis to apply a static two-g signal. Such calibration tests were made just before the runs and just after the runs.

3.6 IMPERFECTIONS IN THE APPARATUS AND THEIR EFFECTS ON THE SHAPES OF THE HYSTERESIS LOOPS

A careful study of the apparatus revealed the possibility of certain

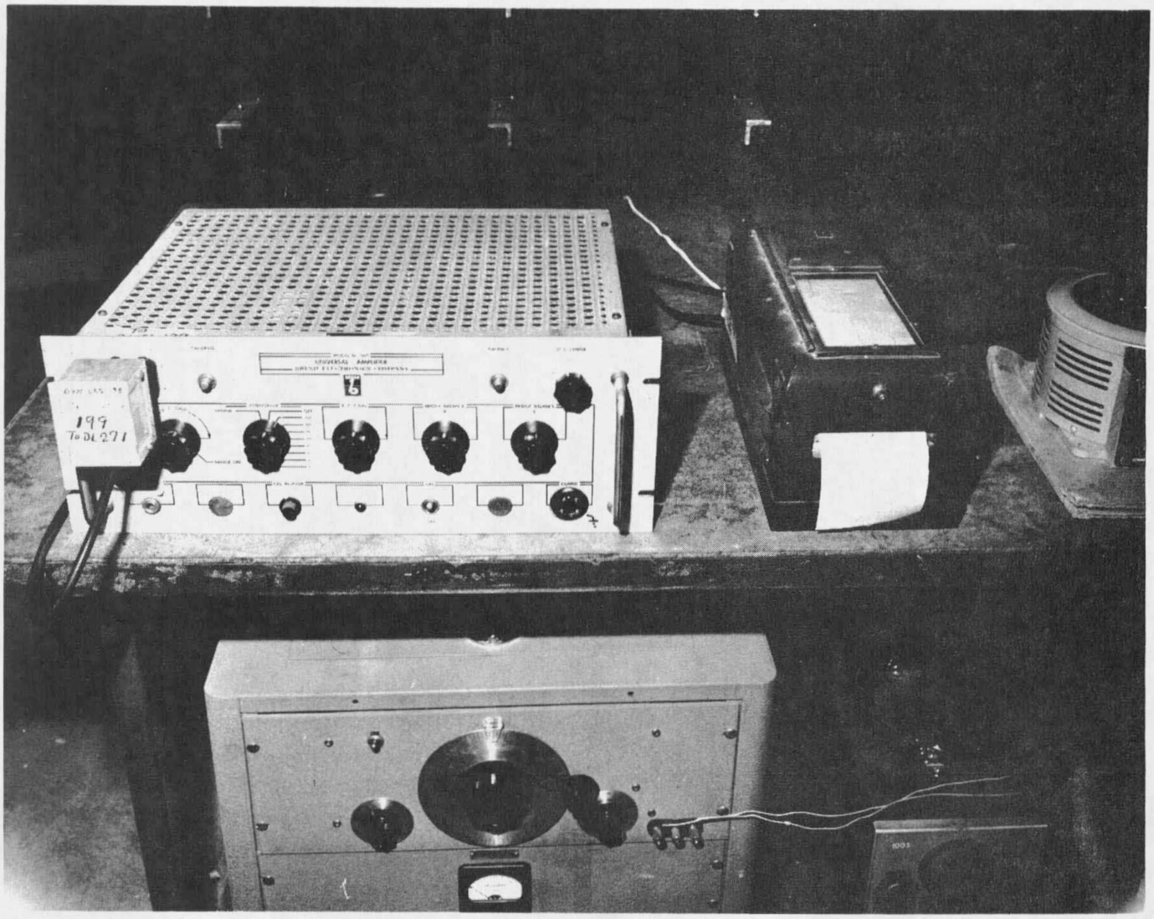

Figure 13: The amplitude recording instruments.

imperfections in its construction influencing the shape of the hysteresis loops. Efforts were made to eliminate these imperfections but it was not possible to remove all of them. This section is devoted to a discussion of the effects of these imperfections in the apparatus.

3.6.1 ROUGHNESS IN THE SURFACE OF THE SHAFTS

The shafts extending from the side plates into the bearings at the ends of the beams were not machined, but rather were made of hot rolled steel in the as-received condition, except for a smoothing with emery paper. The shafts consequently were not perfectly round, but may have contained projections and depressions on their surfaces.

The effects of a projection or a depression on the surface of the shaft on the shape of a hysteresis loop can be demonstrated by taking the representative case of a projection, shown in Figure 14. The end of the bridge is shown resting on a projection of height δ. As the beam is loaded and the shaft rotates, the end of the bridge dismounts from the projection and so the relative deflection of the beam, measured at the centerline, will be decreased by $\frac{\delta}{4}$, provided the other three ends of the bridge are in contact with the circular shafts. If the bridge is sufficiently rigid, so that no twisting of it takes place, the relative deflection at the centerline would be $\frac{\delta}{2}$. Figure 14 shows how the shape of the hysteresis loop might be affected by a small projection on the surface of the shaft.

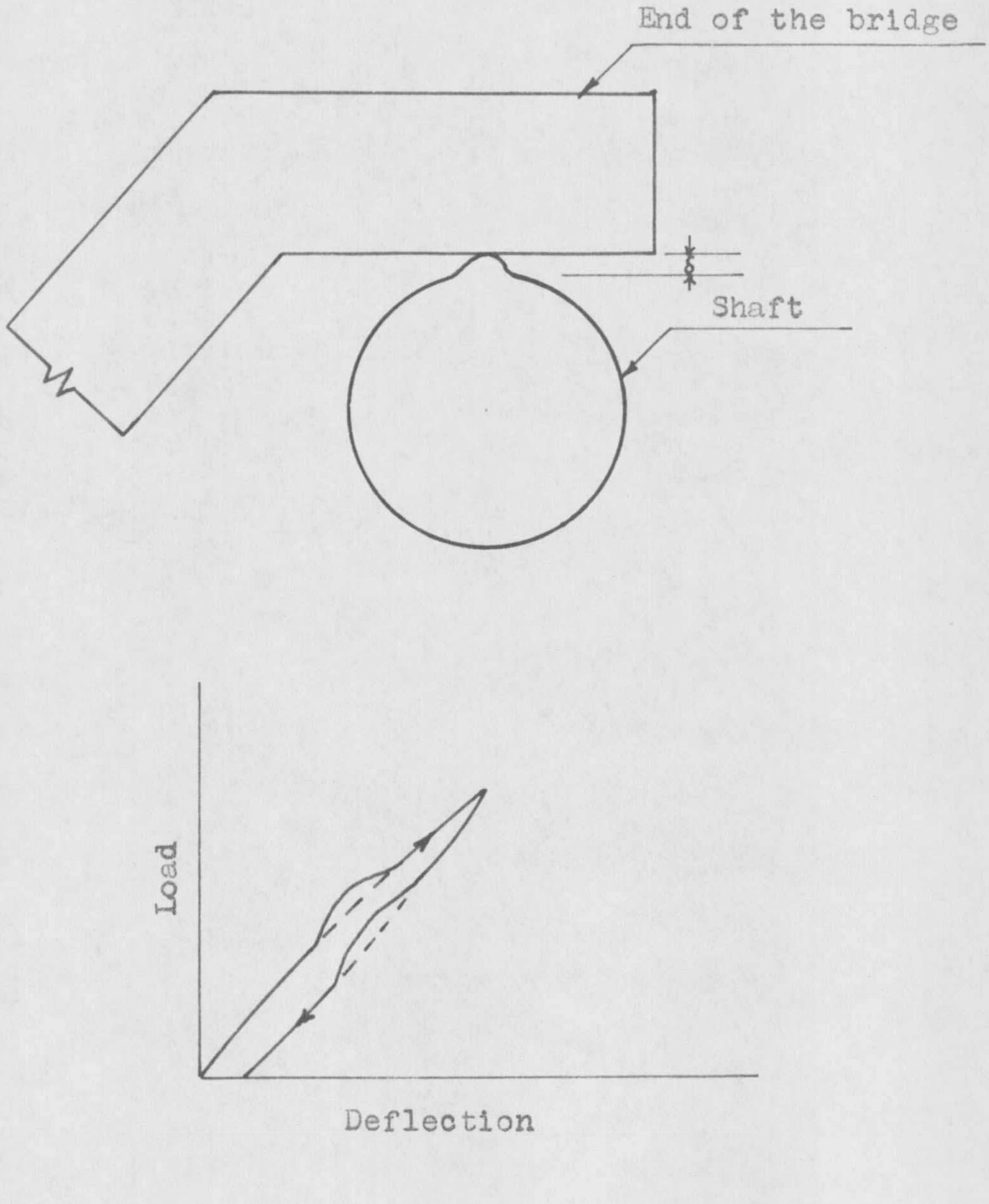

Figure 14: Projection on the surface of the shaft and its effect on the load-deflection curve.

3.6.2 LATERAL MOVEMENT OF THE END OF THE BRIDGE

Movement of the ends of the bridge in the lateral direction of the beam may affect the shapes of the hysteresis loops when the shafts are not perfectly round or when they do not lie in a horizontal plane. Lateral movement either increases or decreases the measured relative deflection of the beam. Lateral movement of the bridge was minimized by placing two cast iron weights, 20 pounds each equidistant from the center. These loads increased the friction between the shafts and the ends of the bridge but it was calculated that the energy loss due to friction was only about 0.012 inch-pound for a cycle of 0.08" amplitude, the maximum amplitude experienced in the tests. This loss is only a fraction of 1% of the losses measured in the beams at this amplitude.

3.6.3 POOR ALIGNMENT OF THE SHAFT

The centerline of the shafts may not be at right angles to the vertical plane containing the longitudinal axis of the beam, as shown in Figure 15. As the beam is loaded, the shafts rotate and so the shafts are displaced vertically. Thus the relative deflection of the beam is either increased or decreased and so the slope of the backbone of the load-deflection curve is changed. To minimize this source of error the shafts were aligned carefully by eye using a small hand-level.

3.6.4 LOADING HEAD NOT PROPERLY CLAMPED

The loading head may not be properly clamped due to a projection either on the surface of beam or on a clamp plate or on both. This

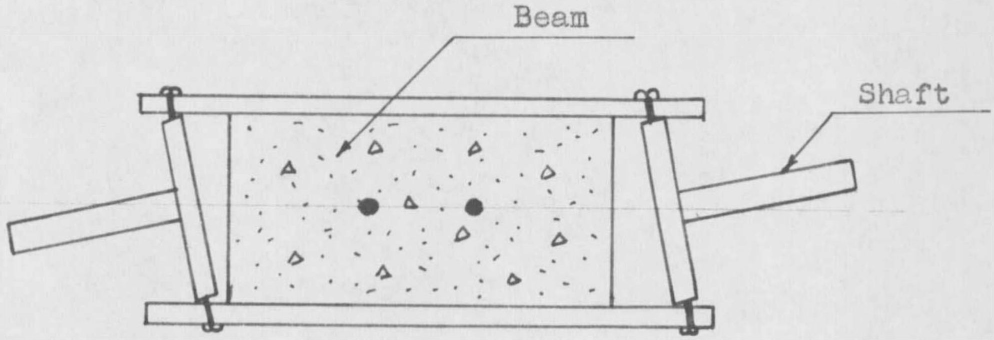

Figure 15: Poor alignment of the shafts.

affects the shape of the hysteresis loop seriously. Figure 16 shows a clamp plate in partial contact with the beam. The effect is to increase the measured relative deflection due to bending of the plate. Figure 16 shows how the shape of the hysteresis loop might be affected in this case.

3.6.5 THE DEFLECTION BRIDGE NOT PARALLEL TO THE BEAM

As the beam is loaded the horizontal projection of the neutral axis shortens. To accommodate this shortening of the neutral axis the ends of the bridge must slide on the shafts. Due to the unequal friction between the ends of the bridge and the shafts, the relative motions of the bridge on the shafts are unequal, which in turn, cause the bridge to move in the longitudinal direction. When the bridge is not horizontal, as shown in Figure 17, this movement of the bridge might either increase or decrease the slope of load-deflection curve. It can be shown that the shortening of the neutral axis for the amplitudes experienced in the tests is very small. The effect of the longitudinal movements of the bridge on load-deflection curves, therefore, was extremely small.

3.7 STATIC TESTING PROCEDURE

Post tensioning of each beam was accomplished within a few hours after the beam was removed from the fog room. Then the surfaces of contact of the beam with the support bearing plates and the loading clamps were made smooth by capping the top and the bottom faces of the beam, at the ends and at the center, with a sulphur compound normally

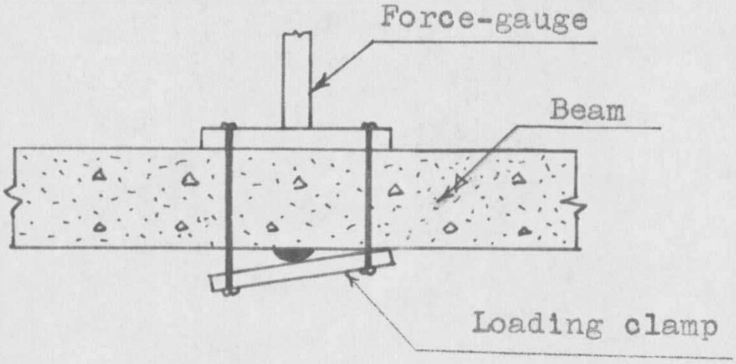

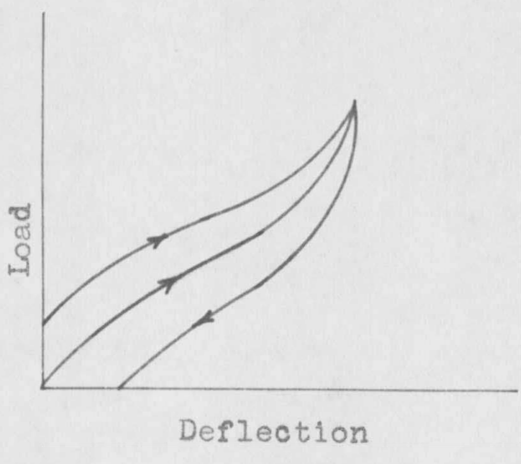

Figure 16: Loading head not properly clamped and its effect on load-deflection curve.

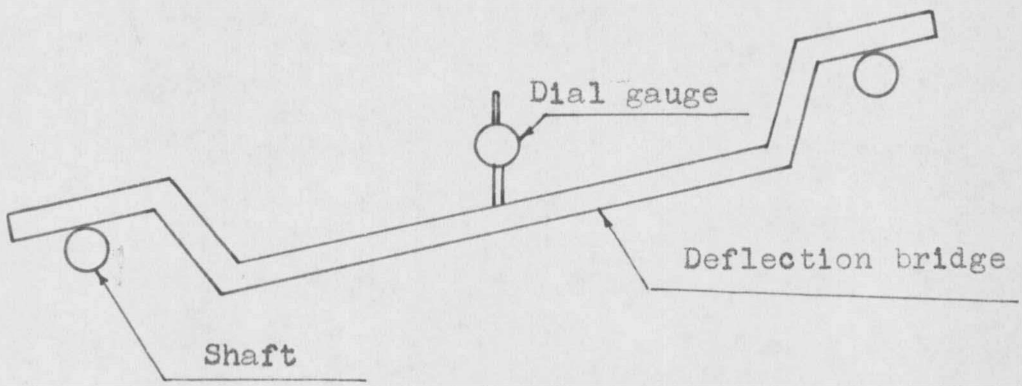

Figure 17: Deflection bridge not parallel to the beam.

used for capping control test cylinders. The beam was then mounted in the loading frame.

The support clamps were made very tight and properly aligned by eye with the aid of a small hand level. The gauges of the loading head were then connected to the SR-4 strain gauge indicator. The loading-head clamps were first kept loose and care was taken to see that they did not touch the beam when the initial reading was taken for the zero-load. After the zero reading was taken, the loading-head clamps were properly aligned and made very tight.

The vertical screw was then moved up or down by rotating the handle extending from the yoke until the initial zero-load reading was indicated by the strain gauge indicator. Then the dial gauge was attached to the deflection bridge exactly below the line of action of the load. The tip of the dial gauge was cemented to the bottom plate of the loading-head clamp with a drop of Duco cement.

The initial reading of deflection gauge was taken at zero-load and then increments of load were applied and corresponding deflection readings were noted. The application of load and the deflection readings were accomplished by one man. The beam was deflected in an incremental manner with an average displacement rate of 0.000167 inch per second. The beam was first deflected upward and then downward to the same magnitude of the deflection from zero-load conditions. After one cycle the beam was brought back to the zero-load conditions. The duration of the load was kept approximately the same for each load-deflection reading. The beam was subjected to cycles of amplitude 0.02", 0.04", 0.06", and

0.08" measured on one side of zero-load deflection. A few beams were also subjected to cycles 0.02" and 0.08" after they were badly cracked.

The load-deflection curve was plotted for each cycle and from the area of the hysteresis loop, measured with a Dietzgen polar planimeter, the equivalent viscous damping ratio was calculated.

3.8 DYNAMIC TESTING PROCEDURE

3.8.1 STEADY STATE TEST

Dynamic tests were conducted on beams 7 and 8 only. The purpose of steady state test was to obtain experimental resonance curves, from the shapes of which equivalent viscous damping ratios could be calculated.

After a beam was mounted in the testing frame, the exciter and the accelerometer were mounted on the beam as shown in Figure 10. After the exciter and the accelerometer were connected to the frequency measuring system and the amplitude recording system, the apparatus was allowed to warm up for 45 minutes before any readings were taken.

The excitation frequency was varied stepwise starting well below the natural frequency of the beam, approximately 23 cycles per second, up to the highest frequency of the motor, approximately 42 cycles per second. Then the excitation frequency was reversed in the same manner from 42 cycles per second to 23 cycles per second. The frequency of excitation was raised by varying the voltage to the motor. The resonant frequency of the beam was very carefully recorded. A sudden jump in the amplitude from the maximum amplitude of the beam, was noticed by slightly increasing the frequency as seen in Figure 28. The resonance curve was plotted and from the ratio of A_1 to A_2, as shown in Figure 28, Appendix E, the equivalent viscous damping ratio was determined (10).

3.8.2 FREE VIBRATION TEST

Free vibration tests were conducted with the same apparatus which was used for the steady state tests. Each beam was excited by a soft pulse which was generated by striking a cotton cylinder mounted at the center of the beam, with a sponge rubber eraser. Decay vibrations were recorded on the oscillograph recorder and the equivalent viscous damping ratio was calculated from the ratio of successive amplitudes, x_o and x_1, as:

$$\zeta_{eq} = -\frac{1}{2\pi}\log\frac{x_1}{x_o}$$

where ζ_{eq} is the equivalent viscous damping ratio.

CHAPTER 4

TEST RESULTS AND DISCUSSION

4.1 TEST RESULTS

The first half of this chapter is devoted to the presentation of the test results determined from the static tests. The following data represent the energy dissipation, ΔE, the stiffness factor, k, and the equivalent viscous damping ratio, ζ_{eq}, for various cycles of deflection for each beam. The values of the k were calculated in the manner shown in Figure 20, Appendix E.

Beam No. 1

Cycles*	0.02"	0.04"	0.06"	0.08"
ΔE**	0.356	-	-	-
k***	8500	-	-	-
ζ_{eq}	0.0167	-	-	-

Beam No. 2

Cycles	0.02"	0.04"	0.06"	0.08"
ΔE	0.448	1.84	3.35	7.17
k	4620	4890	5940	5040
ζ_{eq}	0.0389	0.0374	0.025	0.0351

---

*These numbers represent deflection measured on one side of zero-load deflection.
**Units of ΔE are pound-inches.
***Units of k are pounds per inch of centerline deflection.

Beam No. 3

Cycles	0.02"	0.04"	0.06"	0.08"
ΔE	0.816	1.89	4.02	10.65
k	8480	5370	7510	5940
ζ_{eq}	0.0371	0.0349	0.0238	0.0446

Beam No. 4

Cycles	0.02"	0.04"	0.06"	0.08"
ΔE	0.511	1.473	8.85	11.655
k	11700	11500	19400	8630
ζ_{eq}	0.0174	0.0128	0.0202	0.0335

Beam No. 5

Cycles	0.02"	0.04"	0.06"	0.08"
ΔE	0.574	1.84	8.09	15.10
k	10920	11520	7900	10420
ζ_{eq}	0.0209	0.0159	0.0454	0.0350

Beam No. 6

Cycles	0.02"	0.04"	0.06"	0.08"
ΔE	0.576	1.448	6.06	10.6
k	9100	9950	9760	8640
ζ_{eq}	0.0252	0.0146	0.0275	0.0306

Beam No. 7

Cycles	0.02"	0.04"	0.06"	0.08"
ΔE	0.643	3.03	7.36	11.20
k	12100	13800	9480	6912
ζ_{eq}	0.0212	0.0218	0.0343	0.0401

Beam No. 8

Cycles	0.02"	0.04"	0.06"	0.08"
Δ E	0.882	3.59	7.81	-
k	12080	11800	10980	-
ζ_{eq}	0.0291	0.0303	0.0314	-

Beam No. 9

Cycles	0.02"	0.04"	0.06"	0.08"
Δ E	0.689	1.93	7.36	-
k	11500	11210	10520	-
ζ_{eq}	0.0238	0.0172	0.0312	-

Beam No. 10

Cycles	0.02"	0.04"	0.06"	0.08"
Δ E	0.552	4.60	-	-
k	8060	7190	-	-
ζ_{eq}	0.0273	0.636	-	-

The following are the test results of badly cracked beams. Since the beams were deteriorating slowly, in some cases it was not possible to obtain a closed loop for a cycle and so no energy dissipation could be calculated. In other cases the loop closed before completing the cycle. The following data pertain to closed loops, but incomplete cycle, as shown in Figure 24.

Beam No. 1

Cycles	0.02"	0.08"
ΔE	-	-
k	-	-
ξ_{eq}	-	-

Beam No. 2

Cycles	0.02"	0.08"
ΔE	1.12	-
k	7660	-
ξ_{eq}	0.0704	-

Beam No. 3

Cycles	0.02"	0.08"
ΔE	-	-
k	-	-
ξ_{eq}	-	-

Beam No. 4

Cycles	0.02"	0.08"
E	0.824	-
k	7660	-
eq	0.0524	-

Beam No. 5

Cycles	0.02"	0.08"
ΔE	-	15.85
k	-	8790
ξ_{eq}	-	0.0506

Beam No. 6

Cycles	0.02"	0.08"
ΔE	0.556	5.91
k	8210	7260
ζ_{eq}	0.0356	0.0229

Beam No. 7

Cycles	0.02"	0.08"
ΔE	-	7.92
k	-	6840
ζ_{eq}	-	0.0386

Beam No. 8

Cycles	0.02"	0.08"
ΔE	0.597	-
k	5040	-
ζ_{eq}	0.0572	-

Beam No. 9

Cycles	0.02"	0.08"
ΔE	-	6.64
k	-	7290
ζ_{eq}	-	0.0255

Beam No. 10

Cycles	0.02"	0.08"
ΔE	-	-
k	-	-
ζ_{eq}	-	-

4.2 DISCUSSION OF THE RESULTS

Figures 20 to 26 in Appendix E represent some of the hysteresis loops. Since the shapes of the loops did not differ appreciably among the several beams only a few representative samples are shown.

It is observed from the experimental results that the spring constant, k, varies from beam to beam. It is also observed that there is considerable spread in the values of k for different cycles of the same beam, a 225% variation in Beam No. 4. The variation of k is difficult to explain. It is logically to be expected that as the stress level increases, the value of k should diminish in view of the stress-strain properties of concrete. In some instances, however, the value of k first decreased and then increased as the amplitude of the cycles increased. In other cases, the reverse trend was noticed.

In 1950, at the Massachussetts Institute of Technology (2) tests were conducted on simply supported reinforced concrete beams subjected to reversible static loads. It was observed that there was more than 100% variation in the values of k in identical beams subjected to the same test conditions. No reasons for this variation were given then.

In 1959, Jacobsen (9) discussed these tests and commented on the variation but he did not advance any explanation for it. The reasons for the variation in the values of k in identical beams need further investigation.

One reason which might be advanced for the variation of k for different beams might be imperfections in the apparatus. The imperfections which may have had a major effect on the variation of k are the misalignment of the shafts in the horizontal plane, and the movement of the deflection bridge in the lateral and in the longitudinal direction of the beam. The effect of these imperfections were discussed earlier.

It was suspected that the transverse eccentric application of load had caused twisting of the beam and thus was responsible for the variation of k among the different beams. However, calculations showed that any possible twisting of the beam was so small that it would have practically no effect on the variation of k.

It is observed that the equivalent viscous damping ratio in the prestressed beams as determined from the static tests did not exceed 4% critical. In arriving at this conclusion it was assumed that no measureable energy losses occurred in the support system or in the measuring system of the apparatus. This assumption was confirmed by testing a steel beam, made of two channels 3" deep by 4.1 pounds per foot welded together at the flanges. This steel beam had approximately the same stiffness, $\frac{EI}{L^3}$ as the concrete beams. A hysteresis loop resulting from a static test of the steel beam is shown in Figure 27, Appendix E. It is seen that this hysteresis loop is very narrow, and no energy loss can be detected.

It was observed that minor changes in the support system of the beam changed considerably the equivalent viscous damping ratio determined by steady state vibrations. During one of the tests it was observed that the equivalent damping ratio changed from 3.6% to 5.0%

critical, as seen in Figure 29, Appendix E, due to shifting the shafts $\frac{1}{8}$" in the lateral direction in the bearings and shifting the support clamps $\frac{1}{8}$" in the longitudinal direction. Thus it is apparent that the damping ratios determined from dynamic tests do not accurately represent the energy dissipation in the beam alone. During the dynamic tests it was observed that the support system of the beam was vibrating at nearly half the maximum amplitude of the beam. The maximum equivalent viscous damping ratio measured for the beams 7 and 8 determined by the steady state test and free vibration test was 5.0% critical. A representative sample of free vibration response curves are shown in Figure 30, Appendix E. The equivalent dynamic viscous damping ratio determined for the steel beam was 0.68% critical, determined from the free vibration tests.

It was noticed that the response of the beam suddenly dropped to a low value, from the maximum amplitude when the frequency was slightly increased. No points on the resonance curve could be obtained between these two values. The same phenomenon was noticed while decreasing the frequency. It is believed that the reason for this jump was the fact that the speed-torque characteristic of the motor was not sufficiently steep. Hudson (11) pointed out that if the slope of a motor torque - versus - frequency curve is not greater than the slope of the resonance curve of the structure being excited, a stable steady state condition can not be reached.

CHAPTER 5

CONCLUSIONS AND RECOMMENDATIONS

5.1 CONCLUSIONS

The primary objective of the work described here was to investigate the damping properties of prestressed concrete beams and to learn the technique of making such an investigation. It was hoped that a relationship could be established between static and dynamic damping. However, it was found that the apparatus which was designed for static tests did not function satisfactorily for dynamic tests. Nevertheless some results were obtained and experience was gained which will be valuable to future investigators of the same problem.

The following conclusions are made:

1. In static tests, the equivalent viscous damping ratio of the prestressed concrete beams manufactured for this project, did not exceed 4% critical, even under cyclic loading close to failure.
2. In dynamic tests, the equivalent viscous damping ratio did not exceed 5% critical. It is believed that the response from the support system of the beam influenced this value to a considerable extent.
3. No conclusion could be drawn concerning the effect of the grouting of the prestress cables on damping.
4. Dynamic tests on this apparatus are not feasible without modification of the support system.
5. No conclusions could be drawn concerning the effect of the entrained air and the strength of the concrete on damping.

6. No conclusion could be drawn concerning the energy dissipation in badly cracked beams. In five cases the badly cracked beams dissipated more energy then uncracked beams while in three cases the beams dissipated less energy then uncracked beams.

5.2 RECOMMENDATIONS

The following recommendations are made for further investigation of the problem:

1. The deflection measuring bridge should be replaced by some precise and more sensitive device. The following suggestion may help in the improvement of the deflection measuring device.

A thin piano wire can be stretched on the shafts, as shown in Figure 18, parallel to the neutral axis of the beam, by hanging some weights from the ends of the wire. The movement of a fixed point on the beam, relative to the wire, can be measured with a microscope which can travel in the vertical direction.

2. The load measuring device can be modified by using a load cell with a least unit of measurement equal to one pound.

3. The shafts should be precisely machined so that they are smooth and perfectly circular.

4. A device should be constructed to confirm the proper alignment of the shafts.

5. Further investigation is needed to establish the reason why identical concrete beams exhibit different values of k under the same

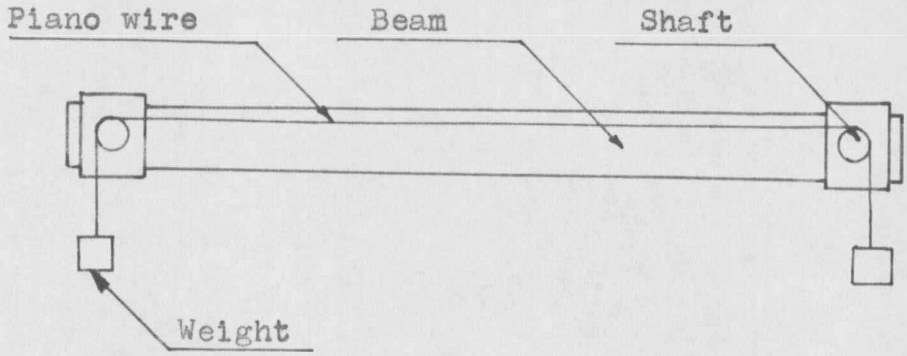

Figure 18: Modified deflection measuring device.

testing conditions.

6. The support system should be modified by increasing the mass and rigidity of the system so that both static and dynamic tests are feasible on the same apparatus.

APPENDIX

APPENDIX A

TABLE II

BEAM PROPERTIES*

Beam No.	f'_c psi	f_c psi	Cross Section	Initial Prestress Condition
1	6000	8660		
2	6000	8660		
3	6000	8160	Constant Beam	Constant Initial
4	6000	8590	Cross-Section	Prestress Condition
5	4000	6660		
6	4000	6775	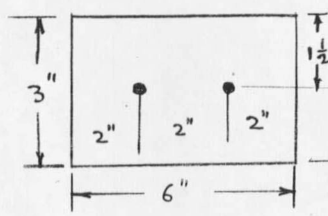	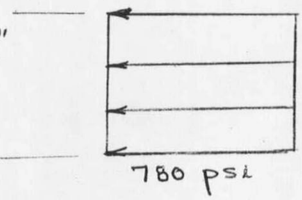
7	4000	6810		
8	4000	6810		
9	4000	6420		
10	4000	6420		

---

*f'_c is the designed ultimate compressive strength of 6" x 12" cylinders after 28 days of moist curing at 70° F.
f_c is the actual ultimate compressive strength of 6" x 12" cylinders, moist curing period varying from 8 to 12 weeks for different beams.

APPENDIX B

CEMENT CHEMICAL ANALYSIS

Ideal Cement Company
Trident, Montana

January 31, 1964

Type I Cement

Chemical Compound	Per cent Of Total	Cement Compound	Per cent Of Total
SiO_2	22.72	C_3S	50.1
Al_2O_3	4.35	C_2S	27.3
Fe_2O_3	3.89	C_3A	4.9
CaO	64.39	C_4AF	11.8
SO_3	1.62		
Loss	1.47	Total	94.1
Total	99.44		

APPENDIX C

AGGREGATE GRADATIONS

Sieve Size	Individual Per cent Retained	Per cent Retained	Per cent Passing
1 inch	0.0	0.0	100.0
$\frac{3}{4}$ inch	9.3	9.3	91.7
$\frac{3}{8}$ inch	61.3	70.6	29.4
No. 4	26.8	97.4	2.6
pan	2.6	100.0	0.0
No. 4	1.0	1.0	99.0
No. 8	14.4	15.4	84.6
No. 16	15.9	31.3	68.7
No. 30	20.5	51.8	48.2
No. 50	30.8	82.6	17.4
No. 100	14.4	97.0	3.0
pan	3.0	100.0	0.0

Fineness modulus of fine aggregate = 2.79

Appendix D

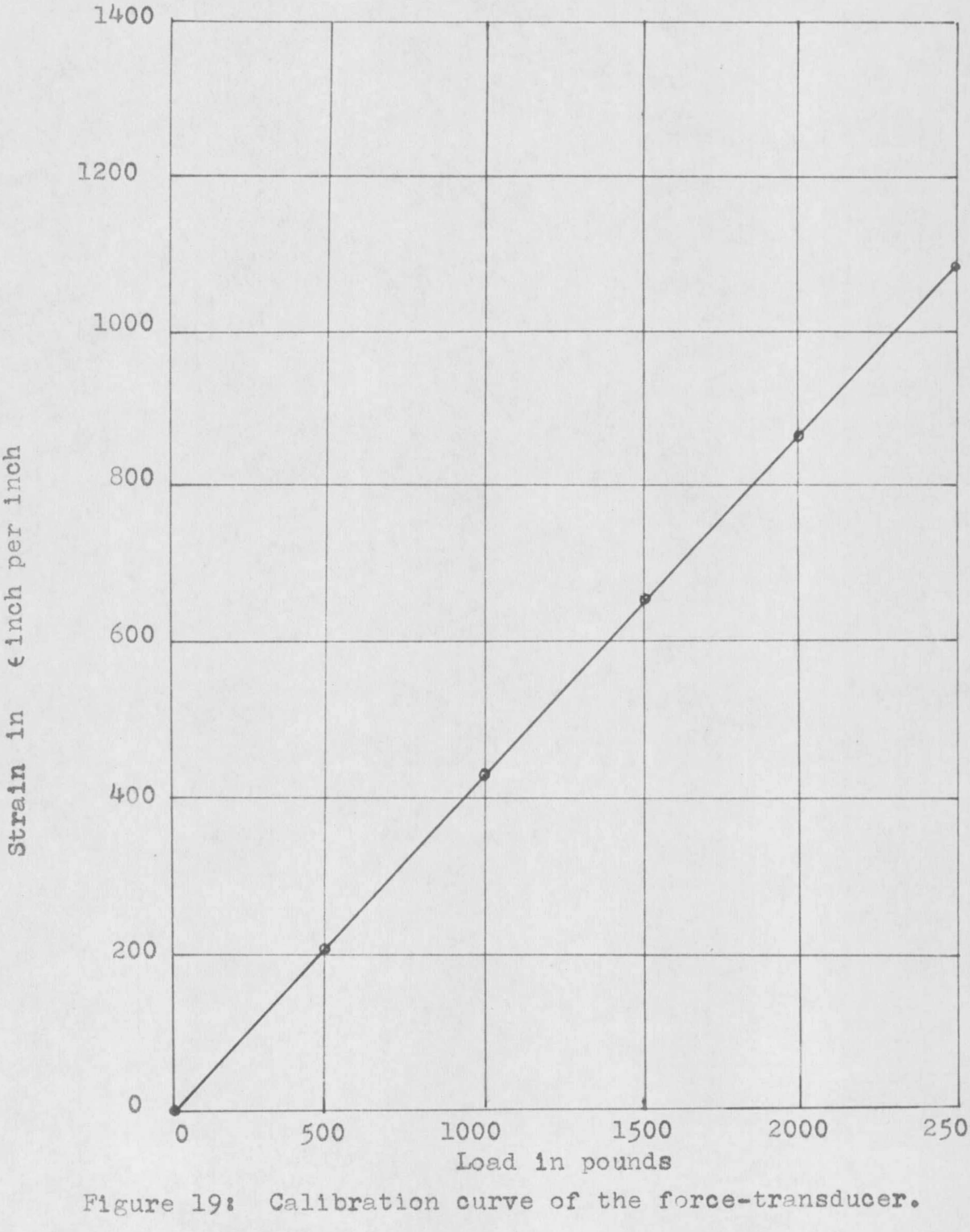

Figure 19: Calibration curve of the force-transducer.

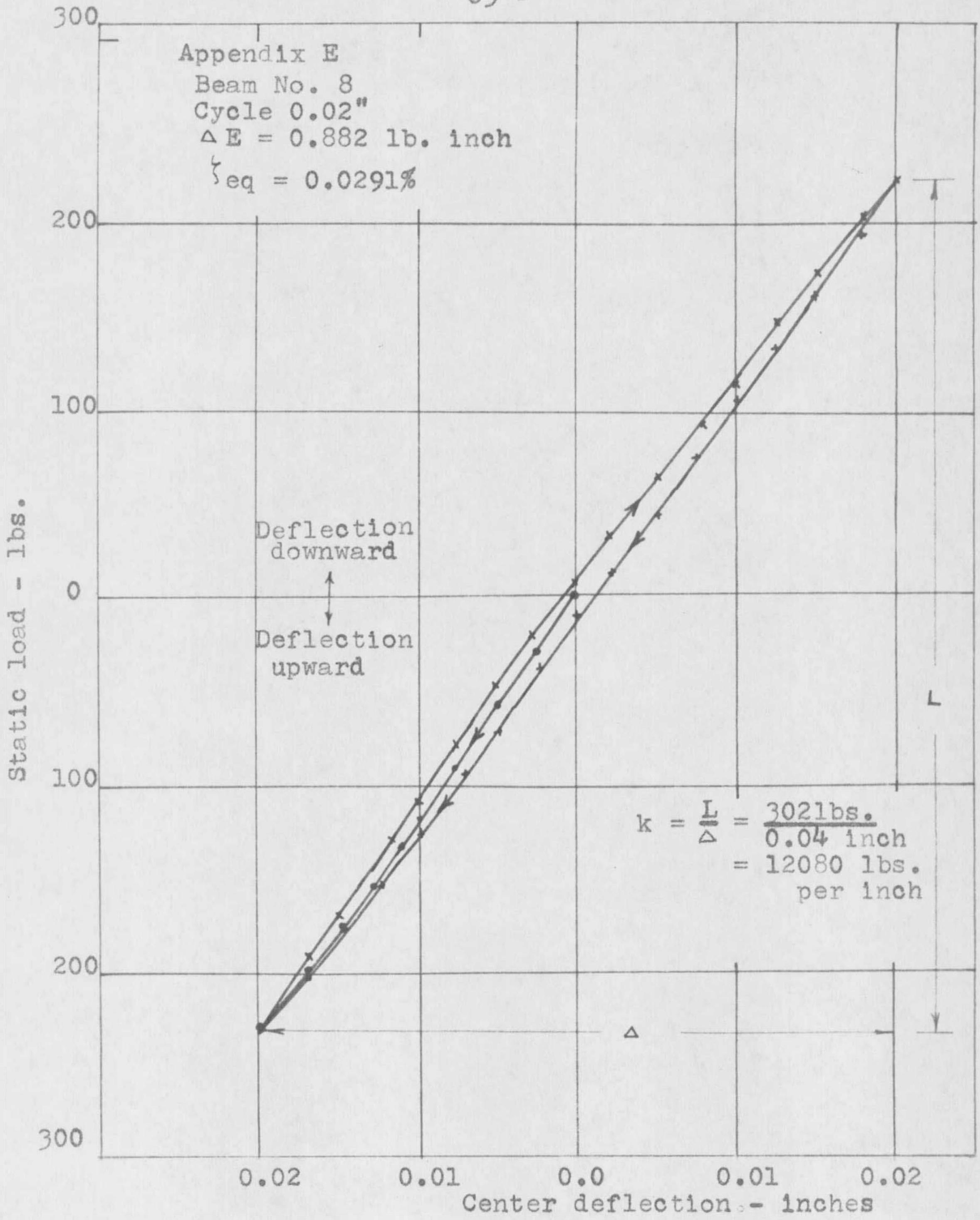

Figure 20: Hysteresis loop

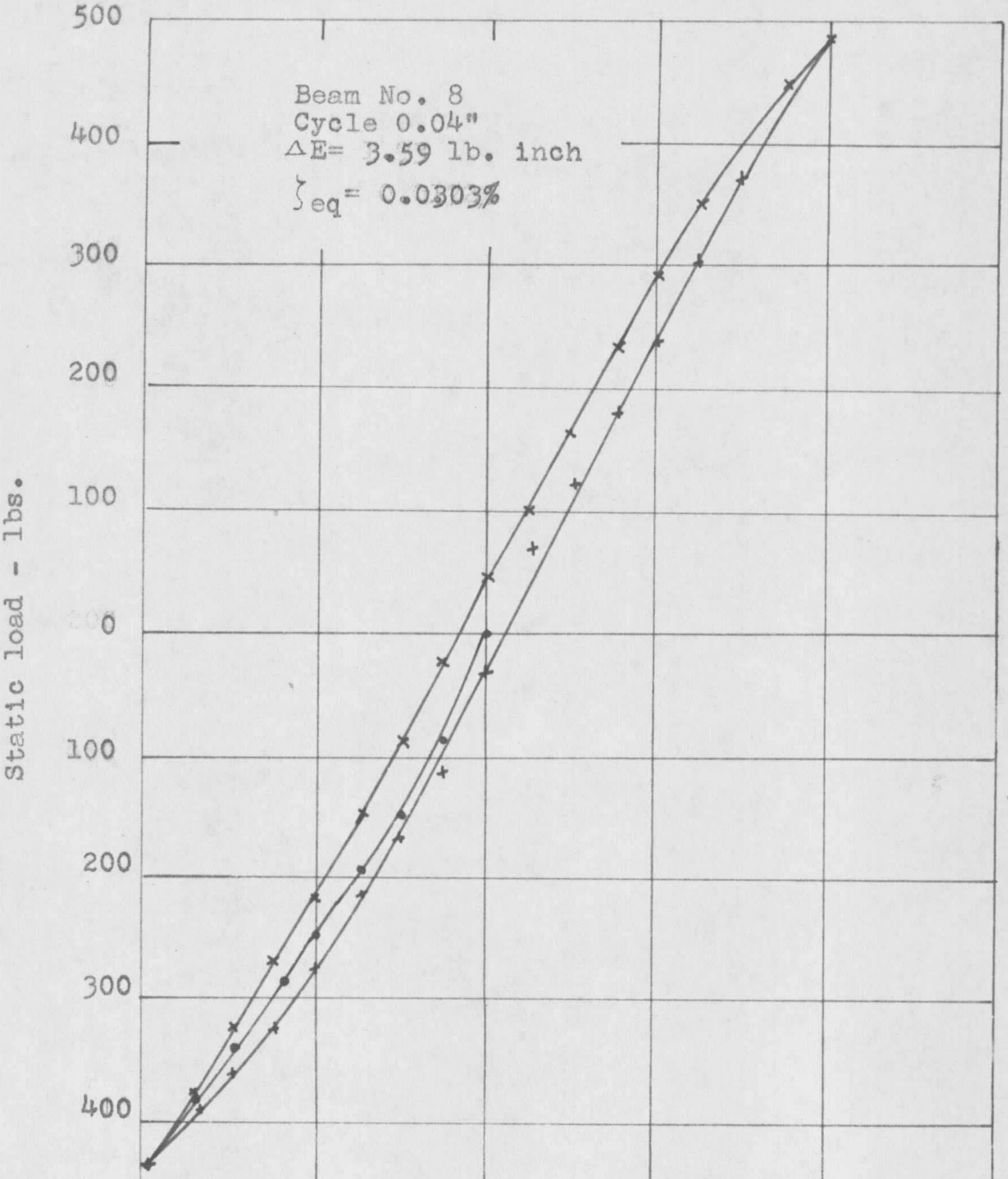

Figure 21 : Hysteresis loop

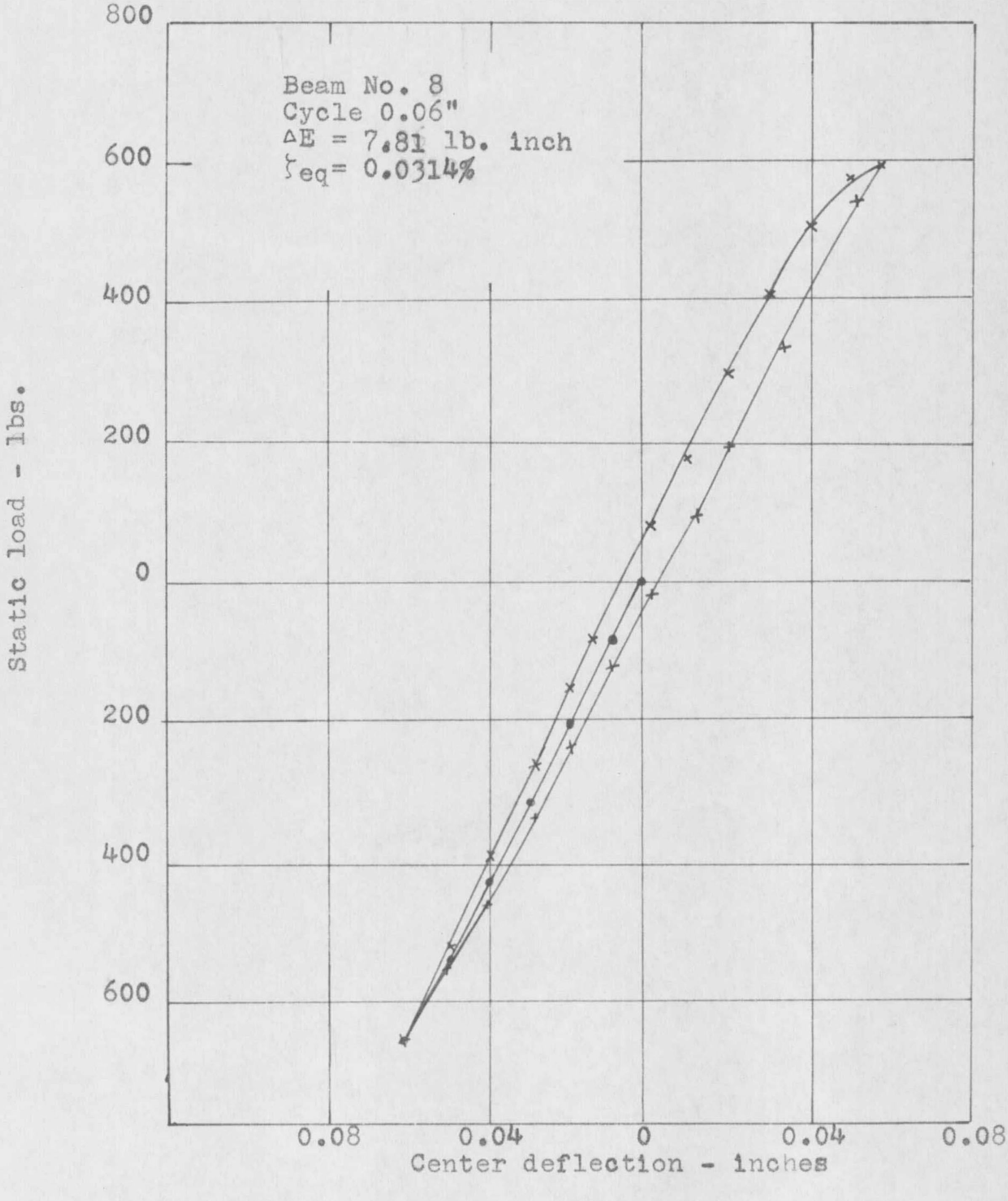

Figure 22: Hysteresis loop

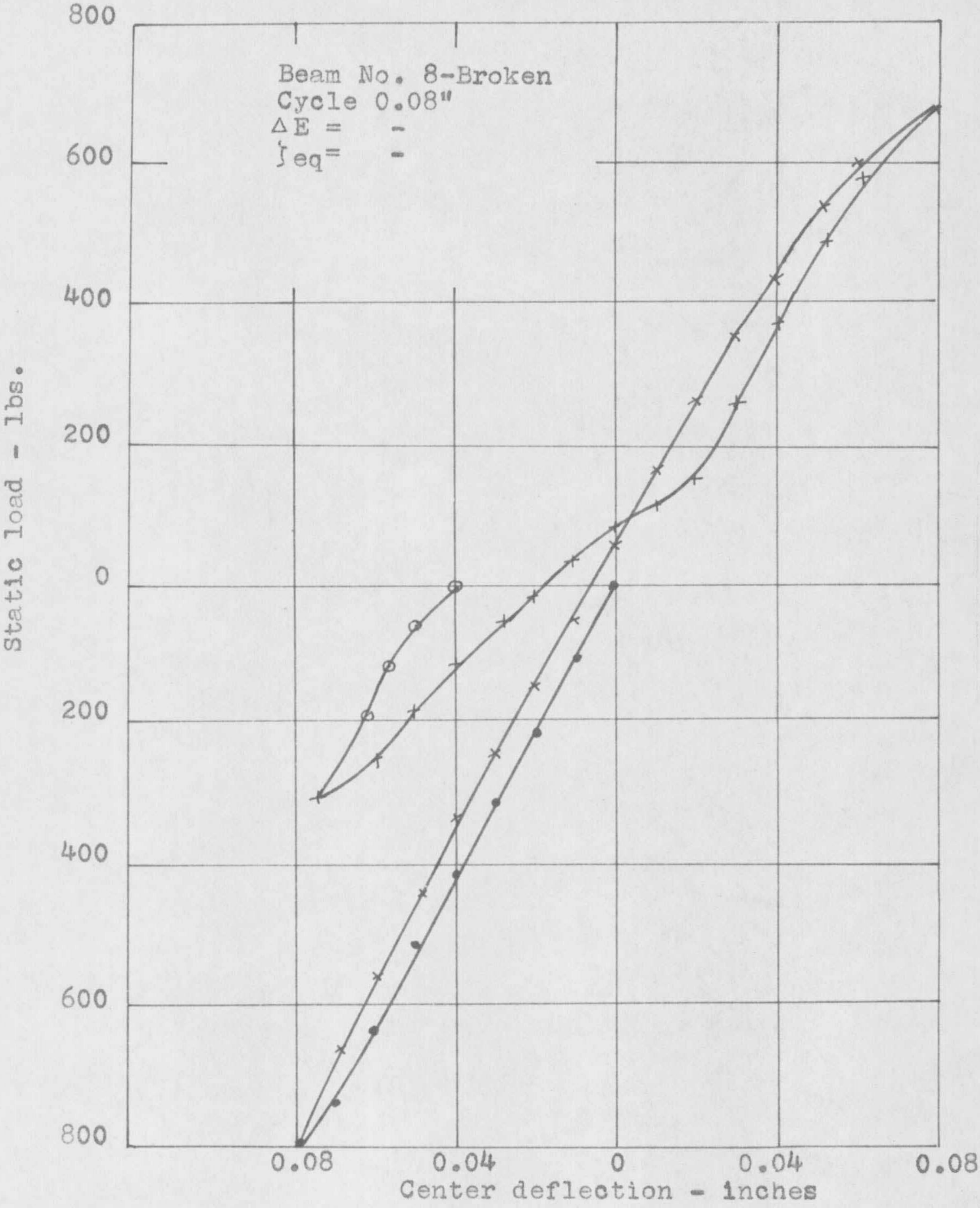

Figure 23: Hysteresis loop

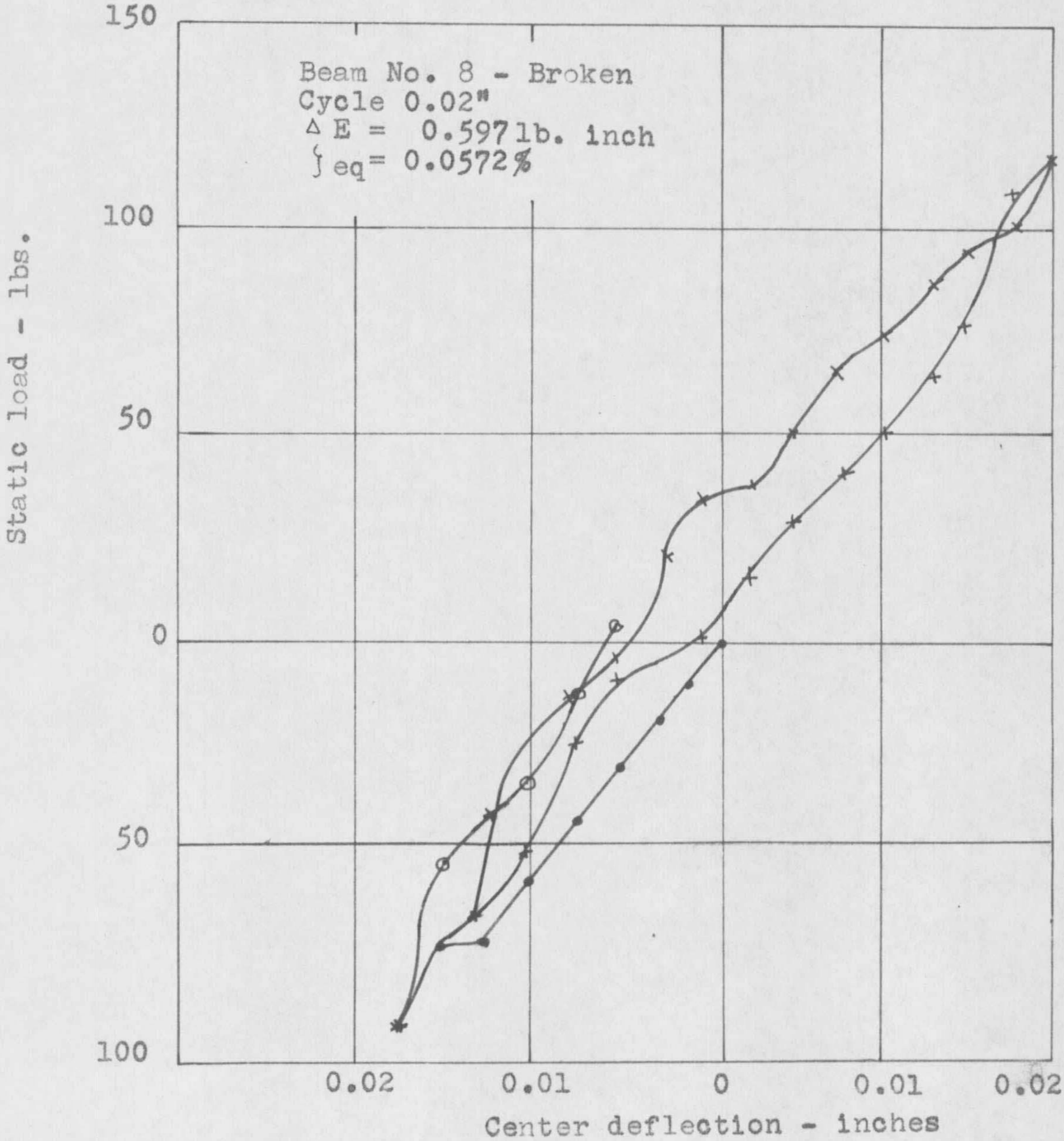

Figure 24: Hysteresis loop

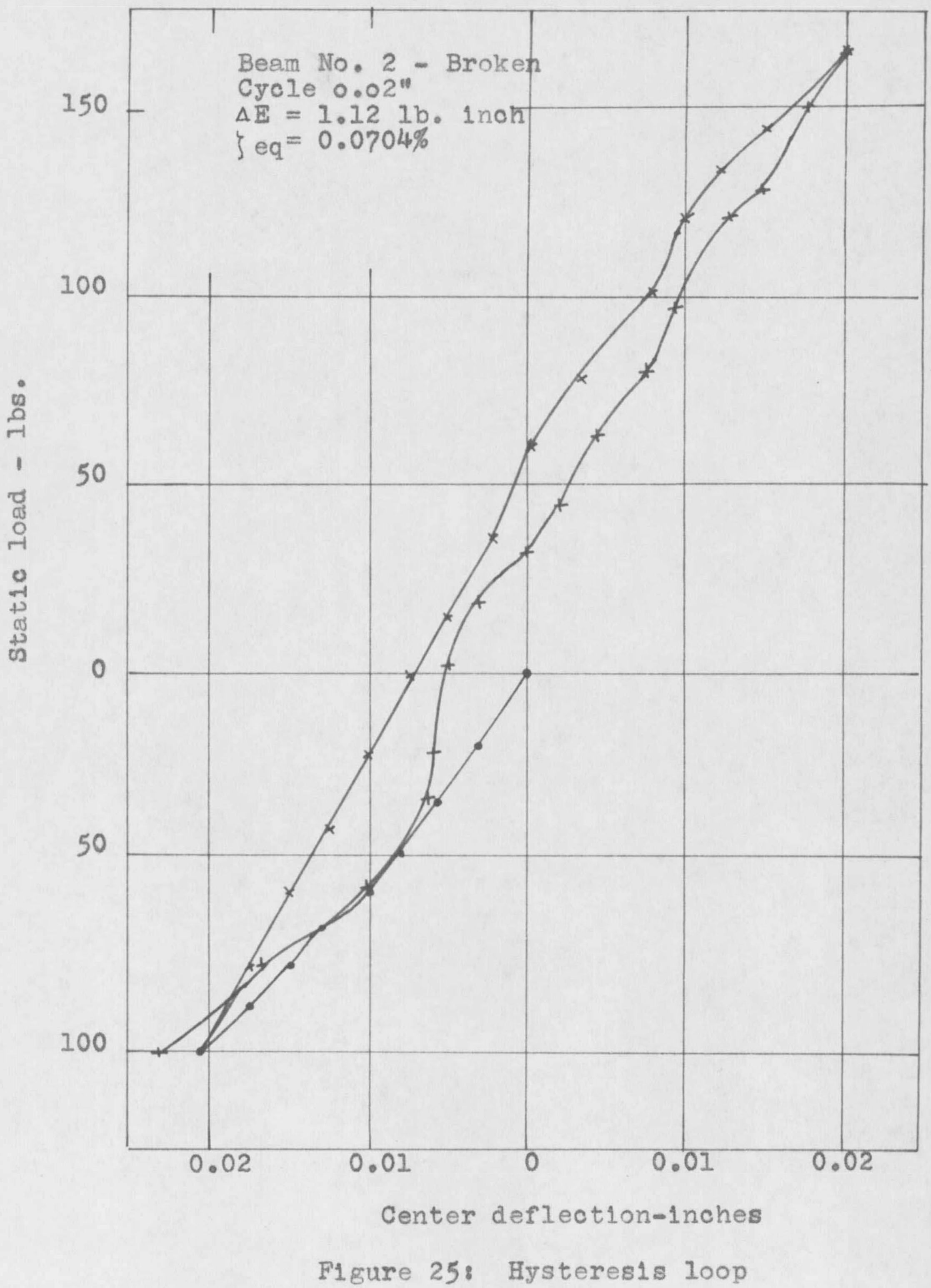

Figure 25: Hysteresis loop

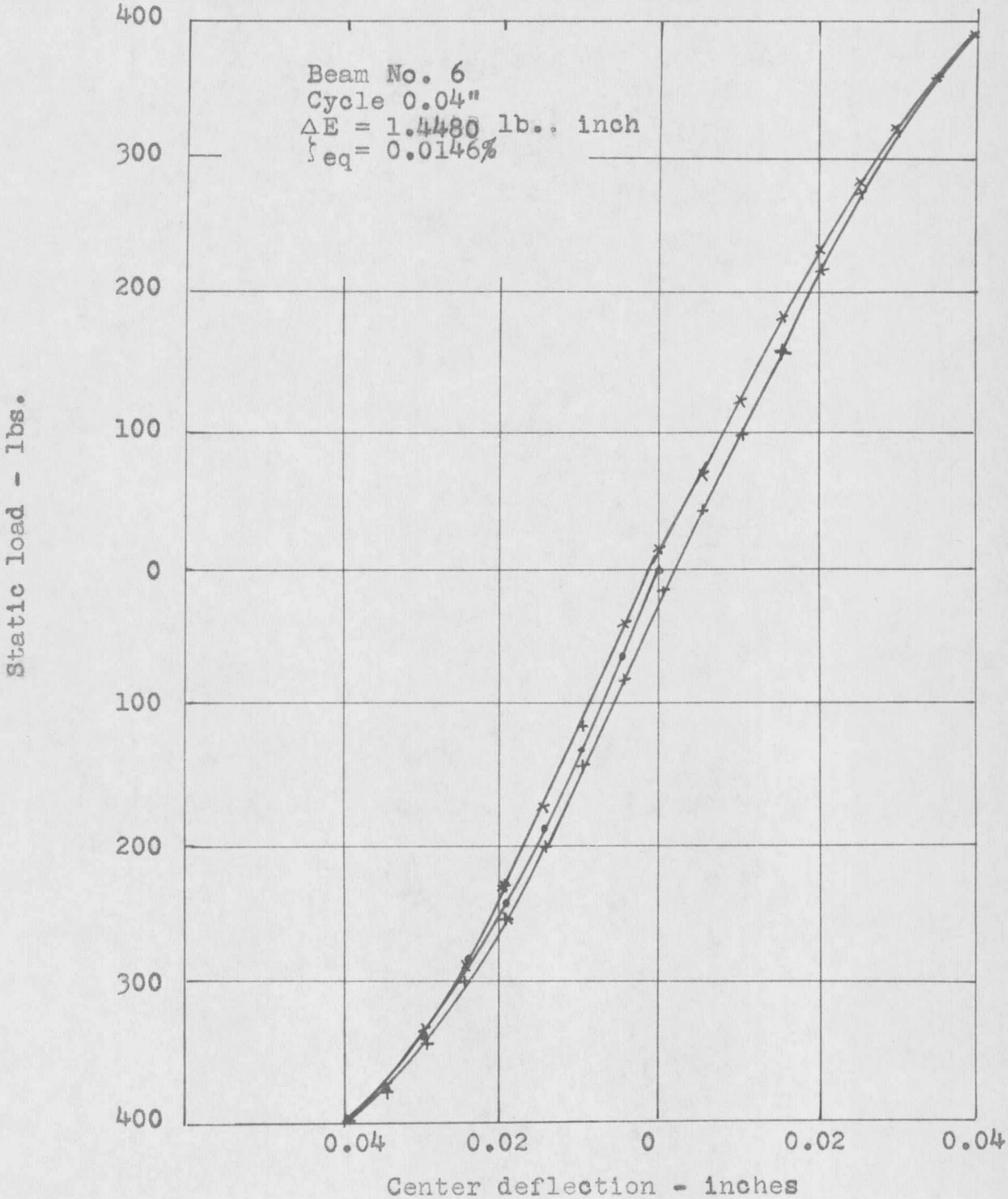

Figure 26: Hysteresis loop

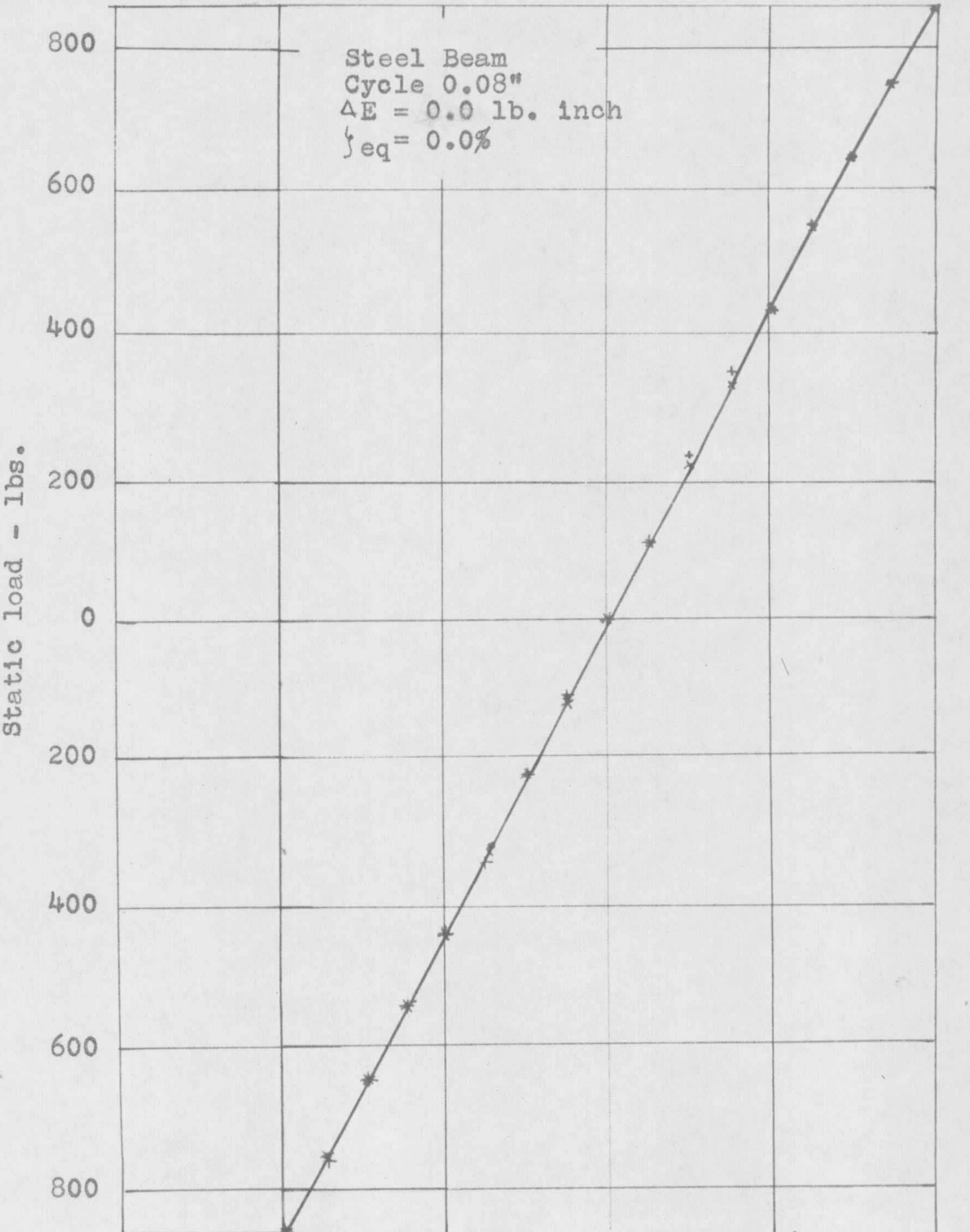

Figure 27: Hysteresis loop

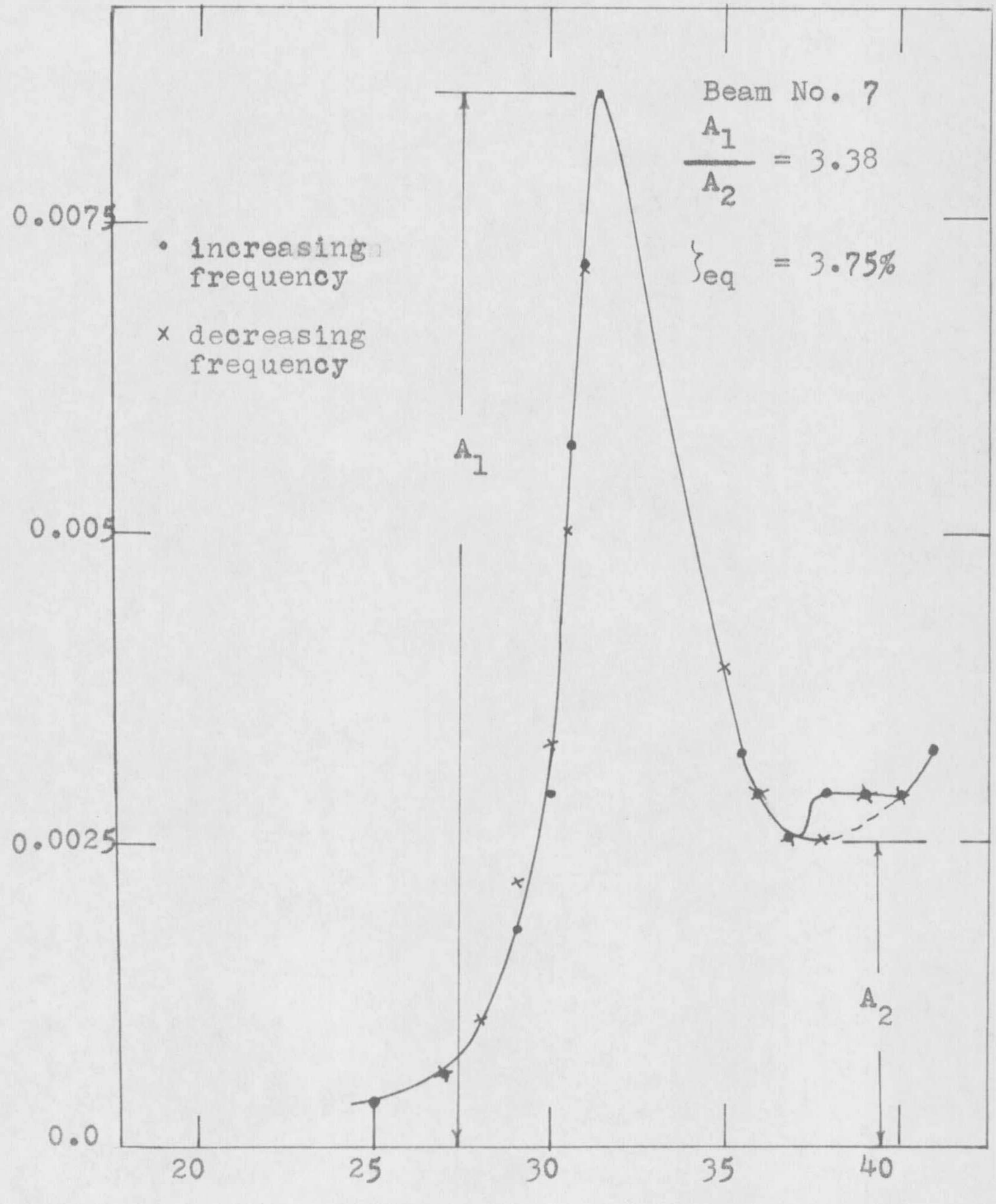

Figure 28: Resonance curve

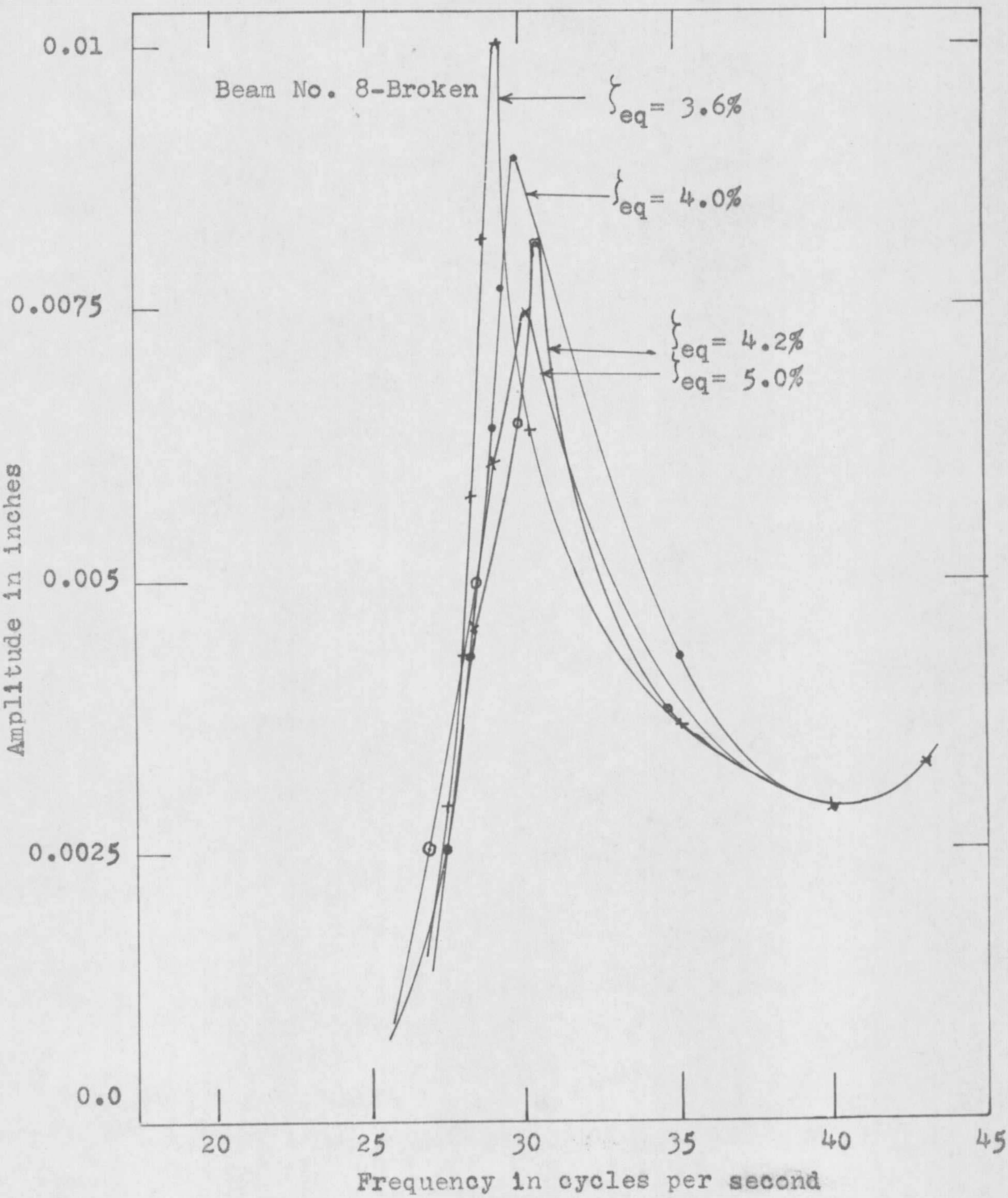

Figure 29: Resonance curve

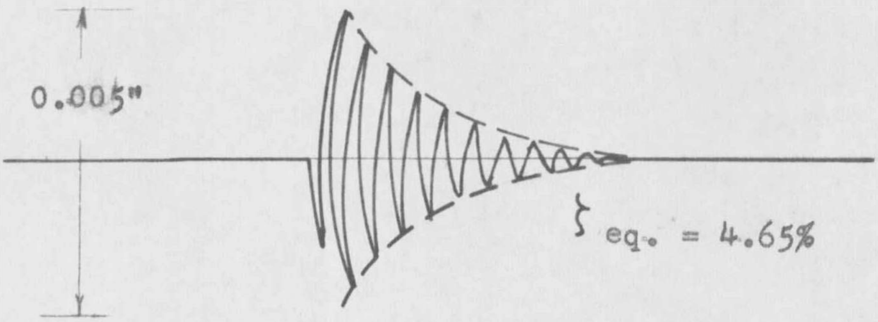

Beam No. 7 Unbroken

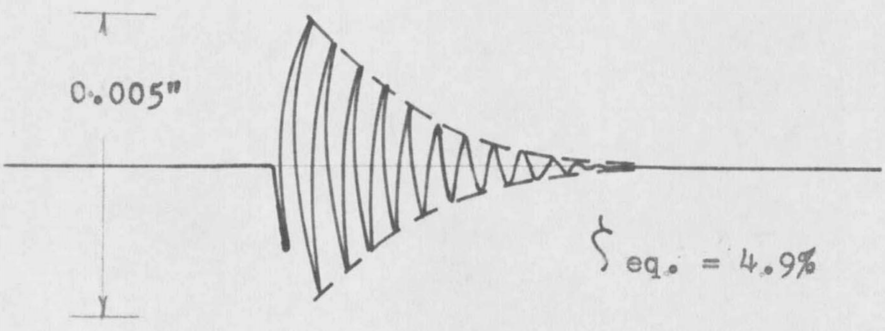

Beam No. 7 Broken

Figure 30: Free Vibration Response

LITERATURE CITED

1. Lazan, B. J., "Energy Dissipation Mechanism in Structures, With Particular Reference to Material Damping." Structural Damping, J. E. Ruzicka, editor, The American Society of Mechanical Engineers, New York 18, New York, (August, 1959), pp. 2-19.

2. "Behaviour of Structural Elements Under Impulsive Loads III" Massachusetts Institute of Technology, Cambridge, Massachusetts, (July, 1951), p. 1.

3. "Blast Load Tests on Post Tensional Concrete Beams", United States Naval Civil Engineering Laboratory, Port Hueneme, California, (May, 1961), p. 23.

4. Penzien, J., "Damping Characteristics of Prestressed Concrete", University of California, Berkeley, California, (January, 1962), pp. 22-23.

5. Tse, F. S., Morse, I. E., Hinkel, R. T., Mechanical Vibrations, Allyn and Bacon, Inc., Boston, 1963, pp. 173-179.

6. Myklestad, N. O., "The Concept of Complex Damping", Journal of Applied Mechanics, Vol. 19, No. 3, 1962, pp. 284-286.

7. Harris, C. M., "Introduction to the Handbook", Shock and Vibration Handbook, Vol. 1, McGraw-Hill Book Company, Inc., New York, 1961, pp. 1-18.

8. Jennings, P. C., "Response of Simple Yielding Structures to Earthquake Excitation", California Institute of Technology, Pasadena, California, (June, 1963), p. 78.

9. Jacobsen, L. W., "Frictional Effects in Composite Structures Subjected to Earthquake Vibrations", State of California, Department of Public Works, Sacramento, California, (March, 1959), p. 30.

10. Keightley, W. O., Housner, G. W., and Hudson, D. E., "Vibration Tests of the Encino Dam Intake Tower", California Institute of Technology, Pasadena, California, (July, 1961), Fig. 17.

11. Hudson, D. E., "Resonance Testing of Full-Scale Structures", Paper presented at ASCE Annual Meeting And Structural Engineering Conference, San Francisco, California, October 7-11, 1963.